FDL-TDR-64-16

FOREWORD

The research work described in this report was performed by the Bell Aerosystems Company, Buffalo, New York for the AF Flight Dynamics Laboratory, Research and Technology Division, Wright-Patterson Air Force Base, Ohio. The work was accomplished under Contract No. AF33(657)-7486, Project No. 8219, Task No. 821901, "Nonlinear Thermoelastic Effects on Hypersonic Stability and Control". Mr. H. M. Davis and Mr. J. E. Jenkins have been the Air Force Project Officers since the initiation of the program in November 1961. The study program was carried out by the Vehicle Structures Department of Bell Aerosystems Company under the Technical Direction of Mr. V. W. Donato and Mr. J. R. Batt.

Results of this program are being presented in a two part report, of which this is Part I Volume 1. Part II presents a method for obtaining hypersonic static aerothermoelastic solutions in the presence of nonlinear aerodynamic and structural behavior and includes data from tests simulating this behavior. A computer program for the solution of nonlinear static aerothermoelastic problems is also presented. This program is available to eligible recipients from the Control Criteria Branch, Flight Control Division, Flight Dynamics, Laboratory, Wright Patterson AFB, Ohio. The results of a feasibility study employing Moire' fringe techniques to measure the angular displacements of practical wing structures are given in FDL-TDR-64-42.

Acknowledgement is given to Messrs. W. Luberacki and F. Braun for their assistance in the computation and preparation of the tables and figures in this report. Appreciation is also expressed to Mr. R. Watkins for the preparation of the digital computer program employed in this part of the study.

ABSTRACT

Linnell's pressure prediction method is used as a basis for developing hypersonic aerodynamic influence coefficient matrices. Matrix inputs are graphically presented, for ten airfoil sections, in Volume 2. The method developed accounts for the nonlinear variation of lifting pressure with angle of attack which is present at hypersonic speeds. Comparisons of theoretical and experimental hypersonic pressure distributions are made.

This technical documentary report has been reviewed and is approved.

W. A. SLOAN, Jr.
Colonel, USAF
Chief, Flight Control Division
AF Flight Dynamics Laboratory

CONTENTS

iv

ILLUSTRATIONS

TABLES

SYMBOLS

c	wing chord
$g = \dfrac{\theta_b}{\tau}$	nondimensional body slope
n	power associated with angle of attack
p	static pressure
q	$\dfrac{1}{2}\rho V^2$, dynamic pressure
q_{n_i}	aerodynamic influence coefficient associated with n^{th} power of angle of attack at the ith reference point, $n = 0, 1, 2,$ or 3.
t	airfoil thickness
t_{max}	maximum airfoil thickness
x,y,z	cartesian coordinate system of axes with origin at leading edge of airfoil
$\dfrac{\triangle p}{q}$	$\dfrac{p_{lower\ surface} - p_{upper\ surface}}{q}$, lifting pressure coefficient
C_p	$\dfrac{p - p_\infty}{q}$ pressure coefficient
$E(\xi)$	function defined in Equation (2.10)
$F_i(\alpha_i)$	arbitrary function of angle of attack defined in Equation (1.2)
$K = M_\infty \tau$	hypersonic similarity parameter based on thickness ratio
$K_e = M_\infty \delta_e$	hypersonic similarity parameter based on expansion flow deflection angle
$K_s = M_\infty \delta_s$	hypersonic similarity parameter based on compression flow deflection angle
$K_\delta = M_\infty \delta$	hypersonic similarity parameter based on flow deflection angle
M	Mach number
P_s	function defined in Equation (2.5)
Q	aerodynamic influence coefficient
S	function defined in Equation (2.10)

SYMBOLS (Cont)

X, Y, Z	Cartesian coordinate system with origin at leading edge of root chord
a_g	geometric or rigid angle of attack defined in Figure 2.1..
$\bar{a} = \dfrac{a}{\tau}$	reduced equilibrium angle of attack
a	equilibrium angle of attack defined in Equation (2.28)
γ	ratio of specific heats
δ	flow deflection angle
$\eta = \dfrac{z}{c\tau} = \dfrac{z}{t_{max}}$	non-dimensional coordinate
$\theta = \dfrac{\delta}{\tau}$	flow deflection angle
θ_b	body slope, surface slope
$\theta_b (0)$	slope at leading edge
ν	expansion wave turning angle
$\xi = \dfrac{x}{c}$	non-dimensional coordinate
$\tau = \dfrac{t_{max}}{c}$	thickness ratio
$\_\wedge\_$	sweep of leading edge
σ	standard deviation

Subscripts

ℓ	lower surface
u	upper surface
s, u	shock condition on upper surface
e, u	expansion condition on upper surface
s, ℓ	shock condition on lower surface
e, ℓ	expansion condition on lower surface
f	flexible case

SYMBOLS (Cont)

$n = 0,1,2,3$	denotes power of angle of attack
i	i^{th} reference point
N	N^{th} reference point
∞	free stream conditions
s	shock conditions
e	expansion conditions

Matrices

$[\ ]$	rectangular matrix
$\lfloor\ \rfloor$	diagonal matrix
$\{\ \}$	column matrix
$\{1\}$	unit column matrix
$\left\{\dfrac{\Delta p}{q}\right\}$	matrix of lifting pressure coefficients
$[Q]$	aerodynamic influence coefficient matrix
$\{\alpha\}$	equilibrium angle of attack distribution
$\lfloor Q_n \rfloor$	aerodynamic influence coefficient matrix associated with n^{th} power of α
$\left[\delta_{\alpha z}\right]$	structural slope influence coefficient matrix

SECTION 1.0
INTRODUCTION

The purpose of the subject study is to extend the technology of hypersonic aerothermoelastic stability and control analysis and test that had been developed under Contract AF33(616)-6653 (References 1-5). The specific requirements of the study were separated into two distinct areas of effort, namely (1) aerodynamics and (2) static aeroelastic solutions and tests. Results of the aeroelastic studies and tests are given in References 6 and 7. The specific requirements of the aerodynamic studies were to develop a method for obtaining hypersonic aerodynamic influence coefficients which extends the region of application of the methods described in Reference 1 and to evaluate this method by comparison with test data.

In order to determine the stability and control characteristics of flexible aircraft, it is necessary to have available analytical methods which account for the redistributed air loads caused by structural flexibility and the attendant changes in equilibrium angle of attack of the flexible aircraft. Analytical methods have been devised which utilize both structural and aerodynamic influence coefficient matrices. These matrices serve as inputs to the static aeroelastic matrix equations which provide a solution for the equilibrium angle of attack under a given set of flight conditions. The equilibrium solutions are then used to obtain the flexible air loads and flexible stability and control derivatives.

In the supersonic speed regime a linear relationship exists between lifting pressure, $\Delta p/q$, and equilibrium angle of attack, α , i.e.,

$$\left\{ \frac{\Delta p}{q} \right\} = \left[Q \right] \left\{ \alpha \right\} \tag{1.1}$$

1

where $\left[Q\right]$ is an aerodynamic influence coefficient matrix.* In direct contrast to the supersonic case, lifting pressure in the hypersonic speed regime is a nonlinear function of the equilibrium angle of attack. Furthermore, the resultant aerodynamic influence coefficient matrices are diagonal matrices since the lifting pressure at a point is a function of only the angle of attack at that point. This phenomena lends itself to simplications in the formulation of lifting pressure relationships and the resultant influence coefficient matrices. The independence of one point from another differs from the supersonic case where the lifting pressure at a reference point is a function of not only the angle of attack at that point but at all other points in the forward Mach cone emanating from the reference point.

It was shown in Reference 1 that hypersonic lifting pressure distributions may be expressed as

$$\left\{\frac{\Delta p}{q}\right\} = \left\{F(\alpha)\right\} \tag{1.2}$$

where, for instance, $\left\{F(\alpha)\right\}$ can be of the form

$$\left\{F(\alpha)\right\} = \left\lfloor Q_1 \right\rfloor \left\{\alpha\right\} + \left\lfloor Q_3 \right\rfloor \left\{\alpha^3\right\} \text{ or}$$

$$\left\{F(\alpha)\right\} = \left\lfloor Q_1 \right\rfloor \left\{\sin\alpha\cos\alpha\right\} \tag{1.3}$$

Further discussions in Reference 5 show that no simple closed form solution (such as is available to the aeroelastician in the supersonic case) for the equilibrium angle of attack can be obtained using Equations (1.3). In order to determine $\left\{\alpha\right\}$, nonlinear methods of analysis are needed. The solution procedures for $\left\{\alpha\right\}$ are further complicated by the fact that nonlinear structural response is being considered in the present study. That is, not one structural slope matrix $\left[\delta_{\alpha Z}\right]$ is used throughout an aeroelastic analysis as in the past but an $\left[\delta_{\alpha Z}\right]$ matrix is used which changes during the interaction process in accordance with the nonlinear behavior being considered. The incorporation of these nonlinear elements in a static aeroelastic analysis are discussed in Part II of this report, Reference 6.

---

* $\left[Q\right]$ is essentially a linear transformation relating the lifting pressure at given reference points to the angles of attack at these same points.

Several methods for determining hypersonic lifting pressure distributions were discussed in Reference 1. If the analyst considers a slender airfoil at high speeds in an inviscid real gas then the lifting pressure function $\{F(\alpha)\}$ takes the form

$$\{F(\alpha)\} = \lfloor Q_0 \rfloor + \lfloor Q_1 \rfloor \{\alpha\} + \lfloor Q_2 \rfloor \{\alpha^2\} + \lfloor Q_3 \rfloor \{\alpha^3\}$$

(1.4)

in accordance with Dorrance's method as discussed in References 1 and 8. Dorrance's method, however, is valid in the range $0 \leq |K_\delta| \leq 1.0$. From a practical standpoint it was found desirable to extend $|K_\delta|$ above 1.0 but retain the same form of $\{F(\alpha)\}$ as given by Equation (1.4). Previous studies showed that Linnell's method (Reference 9) could be written in the form of Equation (1.4). This method is valid in the range $0 \leq |K_\delta| \leq 5.0$. The use of Linnell's original work in developing a method to obtain aerodynamic operators is discussed in the following section.

It is desirable to assess the validity of theoretical methods by comparing their predictions with experimental data. Both Linnell's and Dorrance's methods have been compared with hypersonic pressure data measured on a series of flat, twisted and cambered wing models in Section 4.0 of this report. The test program had been carried out by Grumman Aircraft Engineering Corporation under Contract AF33(616)-6846. Results of this program are discussed in Reference 10.

SECTION 2.0

DESCRIPTION OF LINNELL'S HYPERSONIC
PRESSURE PREDICTION METHOD

2.1   GENERAL

In the previous study, Reference 1, methods for obtaining hypersonic aerodynamic influence coefficients were developed for a given range of $\left| K_\delta \right|$. Specifically, Dorrance's method, valid in the range $0 \leq \left| K_\delta \right| \leq 1.5$, was used to determine influence coefficients in the moderate hypersonic speed regime, $3 \leq M_\infty \leq 15$. Studies showed that Dorrance's method could not be used to extend $\left| K_\delta \right|$ above 1.5 and in fact the true upper limit as discussed in Reference 1 is approximately 1.0. Another method, originally proposed by Linnell, was used to develop lifting pressure relationships in the range $0 \leq \left| K_\delta \right| \leq 5$. However, hypersonic aerodynamic influence coefficients were not developed in Reference 1 using this method. As part of the work on the present study Linnell's method was used as a basis for formulating hypersonic aerodynamic influence coefficients in order to extend the range of $\left| K_\delta \right|$. It is the purpose of the present chapter to discuss Linnell's method as a means for obtaining lifting pressure distributions on slender two-dimensional flexible airfoil configurations at hypersonic speeds.

Before proceeding to the derivation of pressure relationships certain definitions associated with rigid and flexible flow deflection angles must be made. Linnell's method is a function of the rigid flow deflection angle which in turn is a function of the local surface slope and geometric angle of attack. The local surface slope $\theta_b(x)$ is measured with respect to the x axis which joins the leading and trailing edges of the airfoil. The geometric angle of attack, denoted as α_g,

$$\alpha_g = \alpha_{REF} + \alpha_{b_i} + \alpha_{b_t}.$$

α_{REF} is the angle between the relative wind direction and the aircraft reference axis while α_{b_i} is the angle between the aircraft reference axis

4

and some wing reference plane. The third angular component, α_{b_t}, is the angle between the wing reference plane and the x axis. All of these angles are positive in the clockwise direction. The angle α_{b_t} can be visualized, for example, as a built-in structural twist angle.

The rigid flow deflection angle is defined to be the angle between the wind direction and the local tangent to the undeformed airfoil surface. In the case of a flexible airfoil, one additional angle, namely α_s the structural deformation angle, must be considered before the flexible flow deflection angle can be defined. α_s is defined to be the angle between the tangent to the deformed airfoil surface and the tangent to the undeformed airfoil surface and is considered to be positive in the clockwise direction. Basic to the definition of a flexible flow deflection angle is the fundamental structural hypothesis that, "plane sections which are perpendicular to the x axis of an airfoil before deformation remain plane after the airfoil is deformed." This hypothesis allows the analyst to simply add α_s to the rigid flow deflection angle in order to obtain the flexible flow deflection angle. Structurally speaking, the airfoil can be thought to be replaced by the x axis. It is this line which deforms and yields the deformation angle α_s. Physically, the airfoil "wraps itself" around the deformed x axis. Figures 2.2 to 2.4 geometrically describe the flow deflection angles.

In the derivation of the lifting pressure relationships the x axis rather than the mean camber line was chosen in order to facilitate the derivation. (Of course for symmetrical airfoil sections the x axis is the mean camber line.) The choice of the mean camber line presents no problem in the flexible case, nor in the rigid case for that matter, for to obtain the deformed shape, α_s is just added to the upper and lower surface regardless of what reference axis is chosen. As will be subsequently shown the lifting pressure relationships can be derived by only considering the known local surface slopes of the rigid airfoil.

2.2   DISCUSSION OF LINNELL'S METHOD

Linnell's method is thoroughly discussed in References 1 and 9, Reference 9 being Linnell's original work. Another important work, which appeared after

5

Linnell's paper, was performed by Messrs. Eggers, Syverston, and Kraus of NACA (Reference 11). Their work is identical to Linnell's for certain flow conditions and was labeled the "shock-expansion (slender airfoil) method". It is this label which gives the aeroelastician an insight into Linnell's method.

Consider the slender rigid airfoil shown in Figure 2.1.
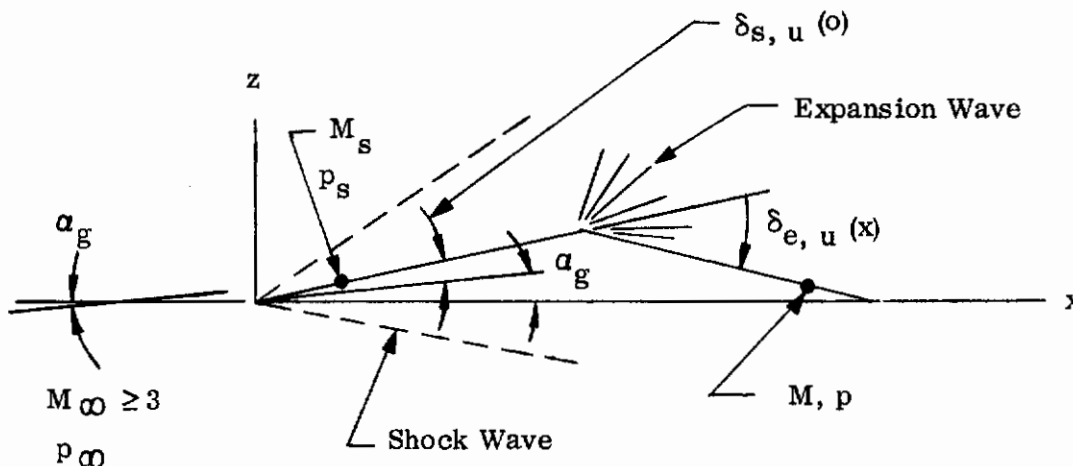
Figure 2.1. Rigid Airfoil Geometry and Physical Relationships

The pressure ratio at any point on the top surface can be obtained from the definition

$$\frac{p}{p_\infty} = \left(\frac{p_s}{p_\infty}\right)\left(\frac{p}{p_s}\right) \tag{2.1}$$

where p_s is the pressure immediately behind the attached shock wave and p is the pressure at the point under study. The pressure ratio (p_s/p_∞) is given by the well-known "tangent-wedge" pressure relationship.

$$\frac{p_s}{p_\infty} = 1 + \frac{\gamma(\gamma+1)}{4} M_\infty^2 \delta_s^2 + \gamma M_\infty^2 \sqrt{\left(\frac{\gamma+1}{4}\right)^2 \delta_s^4 + \frac{\delta_s^2}{M_\infty^2}} \tag{2.2}$$

where δ_s is the shock flow deflection angle as shown in Figure 2.1, Equation (2.2) is derived from the oblique shock equations which are simplified for hypersonic flow. The pressure ratio $\frac{p}{p_s}$ ($\frac{p_e}{p_s}$, for this typical case) is given by the classical "Prandtl-Meyer" expansion relationship and isentropic flow conditions as

6

$$\frac{P_e}{P_s} = \left[1 - \left(\frac{\gamma-1}{2}\right)\left(\frac{M_s}{M_\infty}\right) K_e\right]^{\frac{2\gamma}{\gamma-1}} \tag{2.3}$$

where $K_e = M_\infty \delta_e$, δ_e being the expansion flow deflection angle. The derivation of Equations (2.2) and (2.3) are presented in Reference 1. It is seen that the pressure ratio $\frac{p}{p_\infty}$ is given by the product of the oblique shock and simple wave expansion pressure relationships. Equation (2.1) can be rewritten in coefficient form by use of Equations (2.2), (2.3) and

$$C_p = \frac{2}{\gamma M_\infty^2}\left(\frac{p}{p_\infty} - 1\right) \tag{2.4}$$

as

$$C_p = \left[\delta_s^2 P_s + \frac{2}{\gamma M_\infty^2}\right]\left[1 - \left(\frac{\gamma-1}{2}\right)\left(\frac{M_s}{M_\infty}\right) K_e\right]^{\frac{2\gamma}{\gamma-1}} - \frac{2}{\gamma M_\infty^2} \tag{2.5}$$

where

$$P_s = \left(\frac{\gamma+1}{2}\right) + \sqrt{\left(\frac{\gamma+1}{2}\right)^2 + \frac{4}{K_s^2}}$$

It is noted that for a given airfoil thickness distribution δ_s depends on the angle of attack and leading edge slope only, δ_e varies with x, however. Equation (2.5) is the expression Linnell had derived. It affords a means to compute pressure coefficients on slender rigid airfoil configurations at moderate hypersonic speeds.

In order to use Equation (2.5), certain flow deflection angles need be defined. These angles are those physical quantities through which the air turns to produce an increase or decrease in surface pressure. Since the aeroelastician treats flexible configurations rather than rigid ones flexible flow deflection angles must be defined. It is noted here that in Linnell's method the flow deflection angles need be defined for two cases; namely for the equilibrium angle of attack α less than or equal to the leading edge slope of the upper surface and for α greater than or equal to the leading edge slope of the upper surface. With the aid of Figures 2.2 to 2.4 and the definitions in Section 2.1 the required flexible flow deflection angles can be stated as follows:

7

$(+)$ α_g, α_s

$(+)$ θ_b

$\alpha_s(0)$ — Tangent to Deformed Airfoil at $x = 0$

$\delta_{s,u_f}(0)$

Tangent to Undeformed Airfoil at $x = 0$

$\theta_{b_u}(0) - \alpha_g$

$\overrightarrow{M_\infty}$

$x = 0$

α_g

Free Stream Direction

x

$\theta_{b_u}(0)$

Upper Surface For $0 \leq \alpha(0) \leq \theta_{b_u}(0)$

$\overrightarrow{M_\infty}$

$x = 0$

$\alpha_g = \alpha_{ref} + \alpha_{b_i} + \alpha_t$

$\delta_{s,\ell_f}(0)$

$\alpha_s(0)$

x — Tangent to Deformed Airfoil at $x = 0$

$-\theta_{b_\ell}(0)$

Tangent to Undeformed Airfoil at $x = 0$

$\alpha_s(0) - \theta_{b_\ell}(0)$

Lower Surface for $0 \leq \alpha(0) \leq \theta_{b_u}(0)$
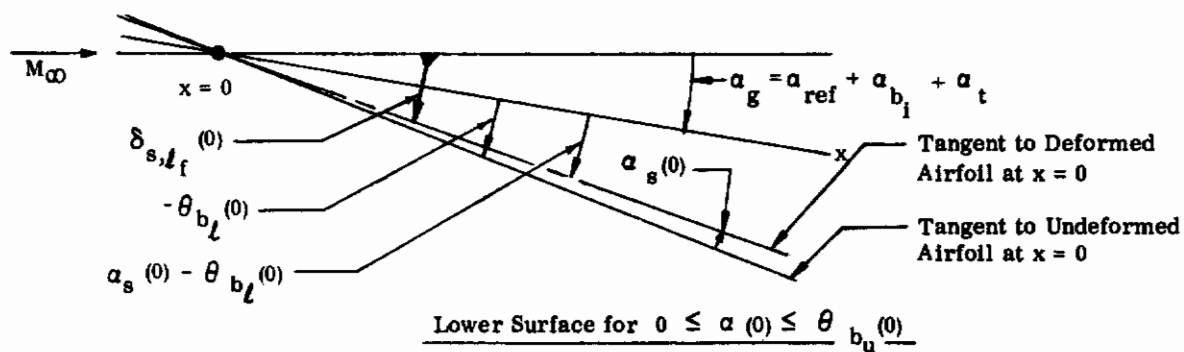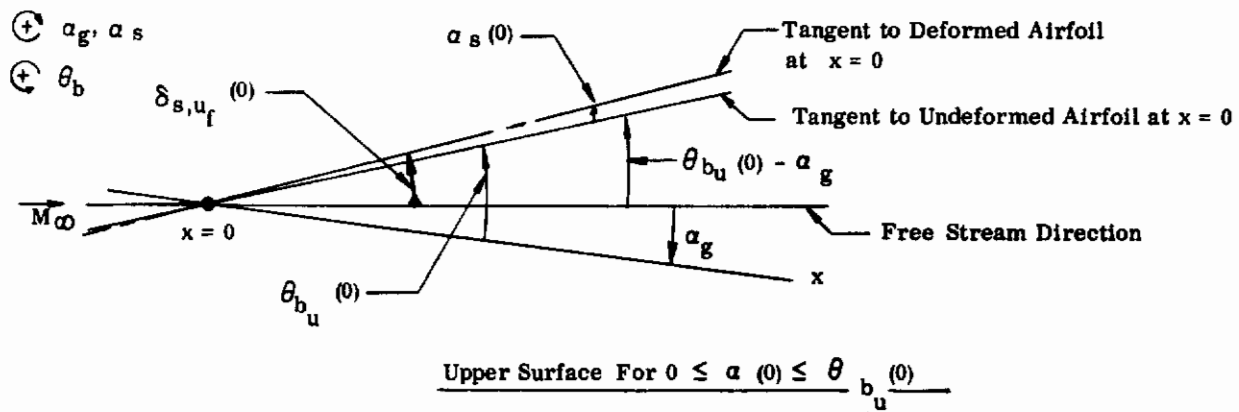
$\delta_{s,u_f}(0) = 0$ (No Shock Wave Present on Upper Surface at $x = 0$ when $\alpha(0) \geq \theta_{b_u}(0)$)

$\delta_{s,\ell_i}(0) = \alpha(0) - \theta_{b_\ell}(0)$ (Same Flow Deflection Angle Since Shock Wave Always Present on the Lower Surface at $x = 0$ Until Shock Detachment Angle Reached)

Both Surfaces for $\alpha(0) \geq \theta_{b_u}(0)$

Figure 2.2. Shock Wave Flow Deflection Angles

8
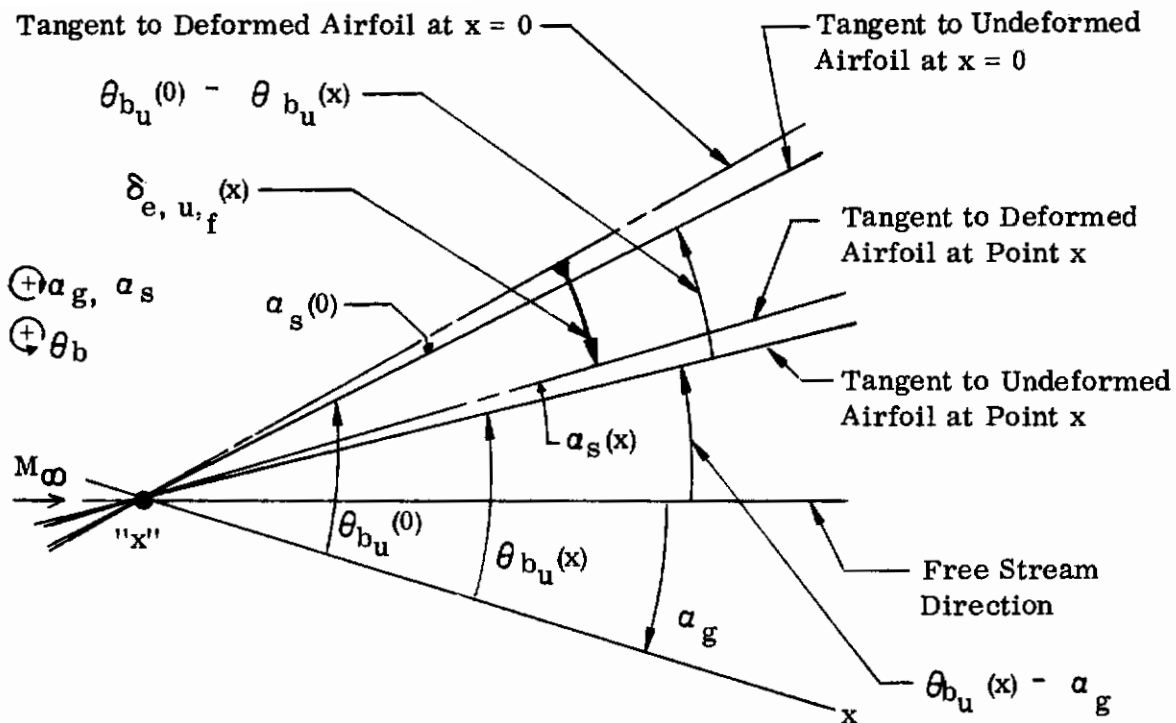
Upper Surface For $0 \leq \alpha(0) \leq \theta_{b_u}(0)$

Upper Surface For $\alpha(0) \geq \theta_{b_u}(0)$

Figure 2.3. Expansion Wave Flow Deflection Angles –
Upper Surface

Flow Deflection Angles

$$\alpha(0) = \alpha_g + \alpha_s(0)$$

$$\alpha_g = \alpha_{ref} + \alpha_{bi} + \alpha_t$$

$\alpha(0)$	Shock	Expansion	Eqs
	Upper Surface		
$0 \le \alpha(0) \le \theta_{b_u}(0)$	$\delta_{s,u_f}(0) = \theta_{b_u}(0) - \alpha(0)$	$\delta_{e,u_f}(x) = \left[\theta_{b_u}(0) - \theta_{b_u}(x)\right] - \left[\alpha(0) - \alpha(x)\right]$	(2.6)
$\alpha(0) \ge \theta_{b_u}(0)$	$\delta_{s,u_f}(0) = 0$	$\delta_{e,u_f}(x) = \alpha(x) - \theta_{b_u}(x)$	
	Lower Surface		
$0 \le \alpha(0) > \theta_{b_u}(0)$	$\delta_{s,\ell_f}(0) = \alpha(0) - \theta_{b_\ell}(0)$	$\delta_{e,\ell_f}(x) = \left[\theta_{b_\ell}(x) - \theta_{b_\ell}(0)\right] - \left[\alpha(x) - \alpha(0)\right]$	(2.7)
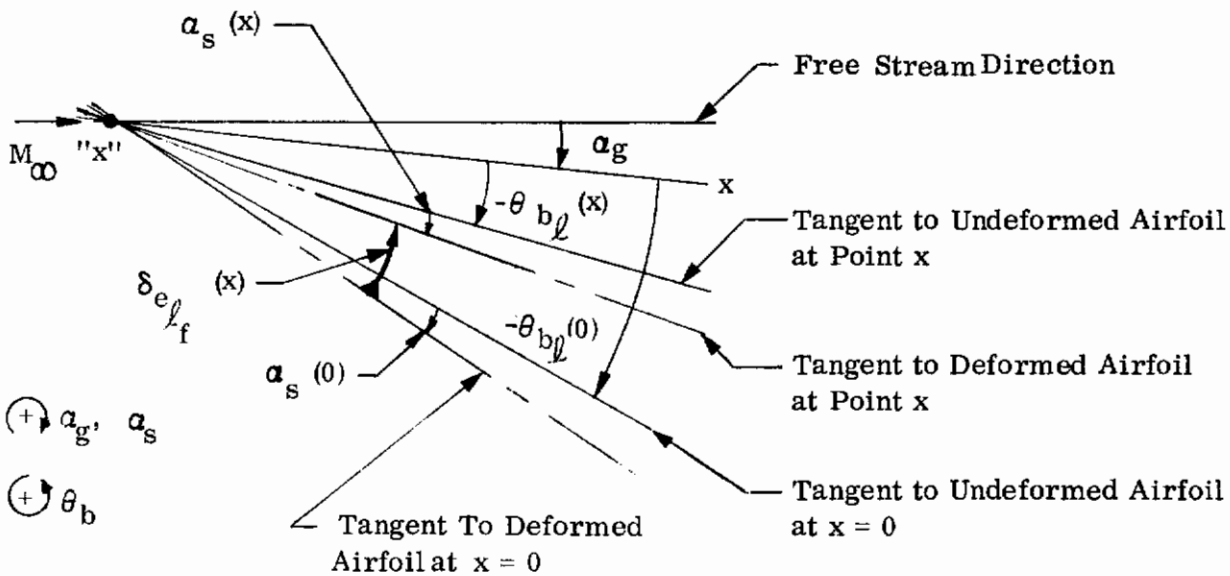
Lower Surface $\alpha(0) \ge 0$

Figure 2.4. Expansion Wave Flow Deflection
Angles - Lower Surface

Two pressure coefficient expressions are obtained for a particular airfoil
shape depending on which set of flow deflection angles are chosen, or better still,
what range of angle of attack the aeroelastician is working in. This state-of-affairs
is detrimental to a static aeroelastic solution since the aeroelastician must "switch
over" to a new set of C_p relationships whenever $\alpha(0) \geq \theta_{b_u}(0)$. In addition, it is
seen from Equations (2.6) and (2.7) that consideration must be given to the value of
the equilibrium angle of attack at the leading edge. Thus another drawback in using
Linnell's method for flexible configurations is that the aeroelastician must have
previous knowledge of the equilibrium angle of attack at the leading edge before a
solution for C_p can be obtained. In a practical situation this information is what the
aeroelastician solves for through the interaction analysis. Means for circumventing
these difficulties have been found and are presented in Section 2.2.2.

The desired lifting pressure expression can be derived by applying
Equation (2.5) to each surface of the airfoil under consideration. In addition the
coordinate system shown in Figure 2.1 can be transformed into a more convenient
nondimensional coordinate system by use of

$$\xi = \frac{x}{c}, \quad \eta = \frac{z}{c\tau} = \frac{z}{t_{max}}, \quad \tau = \frac{t_{max}}{c} \tag{2.8}$$

Also define

$$g(\xi) = \frac{\theta_b}{\tau}, \quad \frac{dz}{dx} = \frac{\tau \, d\eta}{d\xi}$$

$$\theta_f = \frac{\delta f}{\tau}, \quad \bar{\alpha} = \frac{\alpha}{\tau}, \quad K = M_\infty \tau \tag{2.9}$$

Use of Equations (2.8) and (2.9) in Equations (2.5) to (2.7) yields the expression:

$$\frac{C_p}{\tau^2} = S(0) \, E(\xi) - \frac{2}{\gamma K^2} \tag{2.10}$$

11

where

$$S(0) = \theta_{s_f}^2(0) \, P_{s_f} + \frac{2}{\gamma K^2}$$

$$P_{s_f} = \left(\frac{\gamma+1}{2}\right) + \cdot \sqrt{\left(\frac{\gamma+1}{2}\right)^2 + \frac{4}{K^2 \, \theta_{s_f}^2}}$$

$$E(\xi) = \left[1 - \left(\frac{\gamma-1}{2}\right)\left(\frac{M_s}{M_\infty}\right) K \, \theta_{e_f}\right]^{\frac{2\gamma}{\gamma-1}}$$

The flow deflection angles become:

For $\quad 0 \le a(0) \le g_u(0)$

$$\theta_{s,u_f}(0) = g_u(0) - \bar{a}(0), \quad \theta_{e,u_f}(\xi) = \left[g_u(0) - g_u(\xi)\right] - \left[\bar{a}(0) - \bar{a}(\xi)\right]$$

$$\theta_{s,\ell_f}(0) = \bar{a}(0) - g_\ell(0), \quad \theta_{e,\ell_f}(\xi) = \left[g_\ell(\xi) - g_\ell(0)\right] - \left[\bar{a}(\xi) - \bar{a}(0)\right] \tag{2.11}$$

For $\quad \bar{a}(0) \ge g_u(0)$

$$\theta_{s,u_f}(0) = 0, \quad \theta_{e,u_f}(\xi) = \bar{a}(\xi) - g_u(\xi)$$

$$\tag{2.12}$$

$$\theta_{s,\ell_f}(0) = \bar{a}(0) - g_\ell(0), \quad \theta_{e,\ell_f}(\xi) = \left[g_\ell(\xi) - g_\ell(0)\right] - \left[\bar{a}(\xi) - \bar{a}(0)\right]$$

The lifting pressure coefficient can now be obtained by substituting Equation (2.10) into the following expression:

$$\frac{\Delta p/q}{\tau^2} = \frac{C_{p_\ell}}{\tau^2} - \frac{C_{p_u}}{\tau^2} \tag{2.13}$$

or

$$\frac{\Delta p/q}{\tau^2} = S_\ell(0) E_\ell(\xi) - S_u(0) E_u(\xi) \tag{2.14}$$

12

where

$$S_{\ell}(0) = \theta^2_{s,\ell_f}(0)\, P_{s,\ell} + \frac{2}{\gamma K^2}$$

$$S_u(0) = \theta^2_{s,u_f}(0)\, P_{s,u} + \frac{2}{\gamma K^2}$$

$$\theta^2_{s,\ell_f}(0)\, P_{s,\ell} = \left(\frac{\gamma+1}{2}\right)\theta^2_{s,\ell_f}(0) + \sqrt{\left(\frac{\gamma+1}{2}\right)^2 \theta^4_{s,\ell_f}(0) + \frac{4}{K^2}\theta^2_{s,\ell_f}(0)}$$

$$\theta^2_{s,u_f}(0)\, P_{s,u} = \left(\frac{\gamma+1}{2}\right)\theta^2_{s,u_f}(0) + \sqrt{\left(\frac{\gamma+1}{2}\right)^2 \theta^4_{s,u_f}(0) + \frac{4}{K^2}\theta^2_{s,u_f}(0)}$$

$$E_{\ell}(\xi) = \left[1 - \left(\frac{\gamma-1}{2}\right)\left(\frac{M_s}{M_\infty}\right)_{\ell} K\, \theta_{e,\ell_f}(\xi)\right]^{\frac{2\gamma}{\gamma-1}}$$

$$E_u(\xi) = \left[1 - \left(\frac{\gamma-1}{2}\right)\left(\frac{M_s}{M_\infty}\right)_u K\, \theta_{e,u_f}(\xi)\right]^{\frac{2\gamma}{\gamma-1}}$$

The flow deflection angles $\theta_{s,u_f}(0)$, $\theta_{s,\ell_f}(0)$, $\theta_{e,u_f}(\xi)$ and $\theta_{e,\ell_f}(\xi)$ are given by Equations (2.11) and (2.12). Note, when $\left[\left(\frac{\gamma-1}{2}\right)\left(\frac{M_s}{M_\infty}\right) K\, \theta_{e_f}(\xi)\right] \geq$ 1, the terms $E_u(\xi)$ and $E_{\ell}(\xi)$ should be set equal to zero.

The Mach number ratio in Equations (2.10) and (2.14) is given by

$$\left(\frac{M_s}{M_\infty}\right)^2 = \frac{(\gamma+1)\left(\frac{P_s}{P_\infty}\right) + (\gamma-1)}{\left(\frac{P_s}{P_\infty}\right)\left[(\gamma-1)\left(\frac{P_s}{P_\infty}\right) + (\gamma+1)\right]} - \frac{2}{M_\infty^2}\frac{\left[\left(\frac{P_s}{P_\infty}\right)^2 - 1\right]}{\left(\frac{P_s}{P_\infty}\right)\left[(\gamma-1)\left(\frac{P_s}{P_\infty}\right) + (\gamma+1)\right]} \qquad (2.15)$$

13

If the Mach number is sufficiently high the second term in Equation (2.15) can be neglected, then

$$\left(\frac{M_s}{M_\infty}\right)^2 = \frac{(\gamma+1)\left(\frac{p_s}{p_\infty}\right) + (\gamma-1)}{\left(\frac{p_s}{p_\infty}\right)\left[(\gamma-1)\left(\frac{p_s}{p_\infty}\right) + (\gamma+1)\right]} \qquad (2.16)$$

Figure 2.5 shows plots of Equations (2.15) and (2.16) for various Mach numbers. It can be seen from this figure that the second term in Equation (2.15) does not become negligible until $M_\infty \approx 15.0$. However, no mention has been made of the maximum pressure ratios expected when Linnell's method is used. First, it must be recalled that in the derivation of the tangent-wedge pressure relationship, the assumption $\tan^2 \delta_s \approx \delta_s^2$ is made. This means that $\delta_{s_{max}} \approx 15°$. Using this condition in the tangent wedge pressure relationship yields

$$\left(\frac{p_s}{p_\infty}\right)_{max} = 0.0580\, M_\infty^2 + 0.370\, M_\infty^2 \sqrt{0.0247 + M_\infty^{-2}} + 1.00. \qquad (2.17)$$

Use of Equation (2.17) in Equations (2.15) and (2.16) gives the results shown in Figure 2.6. It is seen that for the maximum pressure ratios permissible at each Mach number the differences between Equations (2.15) and (2.16) are not large and in fact decrease to zero when $\left(\frac{p_s}{p_\infty}\right) < \left(\frac{p_s}{p_\infty}\right)_{max}$. Another evaluation of Equation (2.15) and (2.16) is shown in Figure 2.7. In this figure the lifting pressure on a rigid half-diamond airfoil, in the interval $0.50 \le \frac{x}{c} \le 1.00$ was computed for various Mach numbers using Equations (2.14), to (2.16). The differences obtained using Equation (2.15) or Equation (2.16) are insignificant at the lower Mach numbers. At the higher Mach numbers the results are identical. From the above discussion, it can be concluded that small differences in the Mach number ratio give rise to smaller differences in the lifting pressure function. For the purposes of this study Equation (2.16) will be used to determine the Mach number ratios. In closing this particular discussion, it is noteworthy to point out a mathematical error in Linnell's original paper. An expression for the Mach number ratio is

14
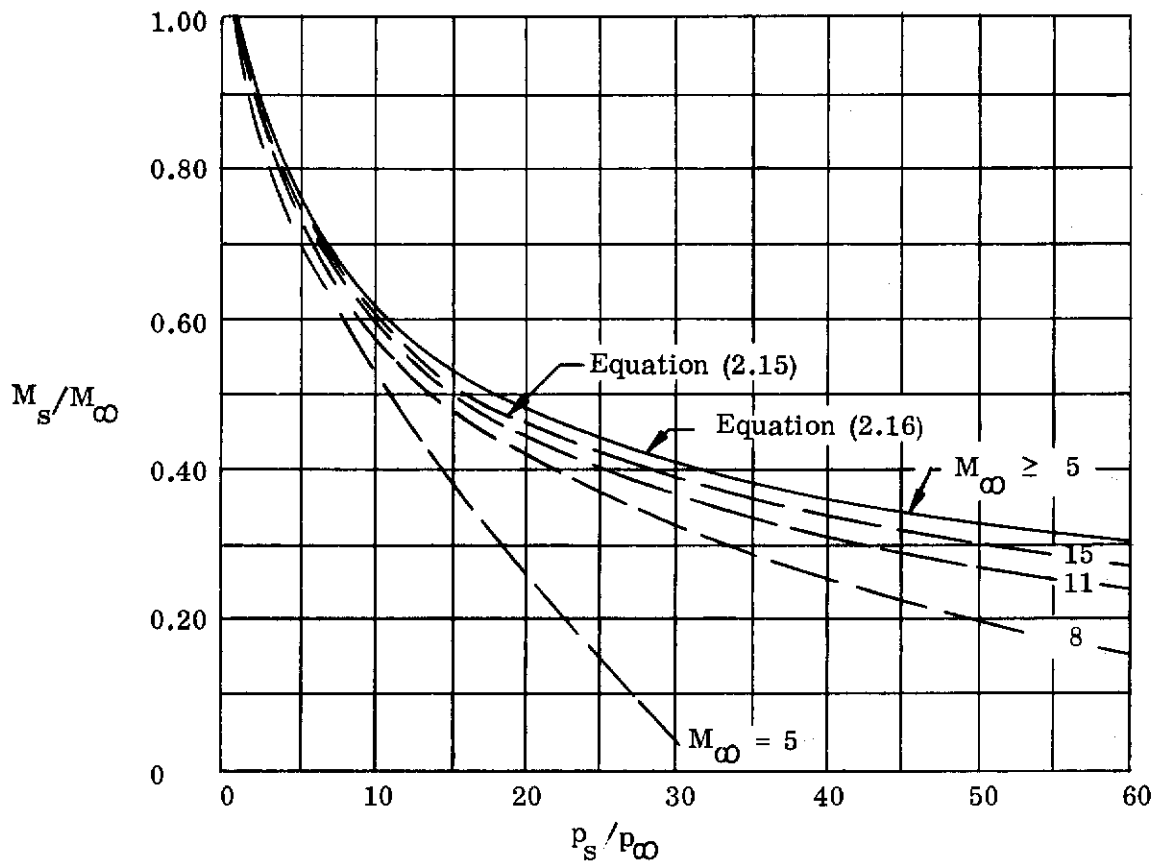
Figure 2.5 Mach Number Ratio

Figure 2.6 Maximum Mach Number Ratio

15

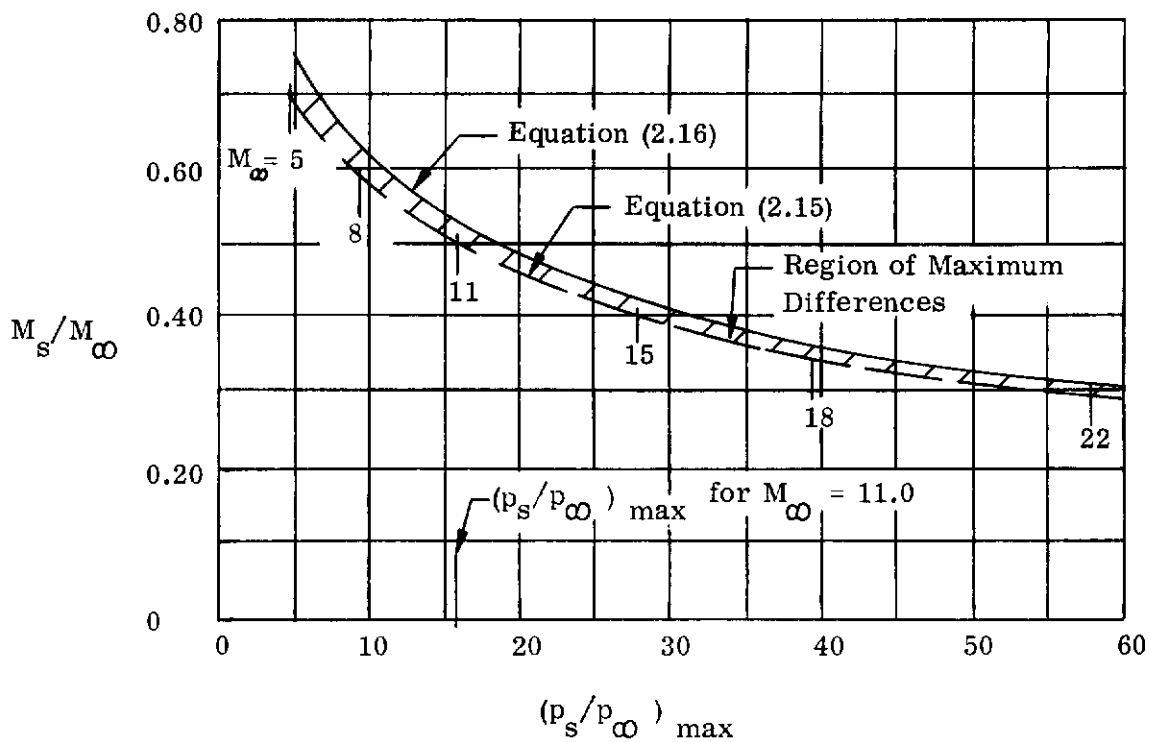| Case	α_g	τ	$\theta_{b_u}(0)$	$\delta_{s,u}(0)$	$\delta_{s,\ell}(0)$
1	5°	0.175	20°	15°	5°
2	5°	0.100	11°	6°	5°

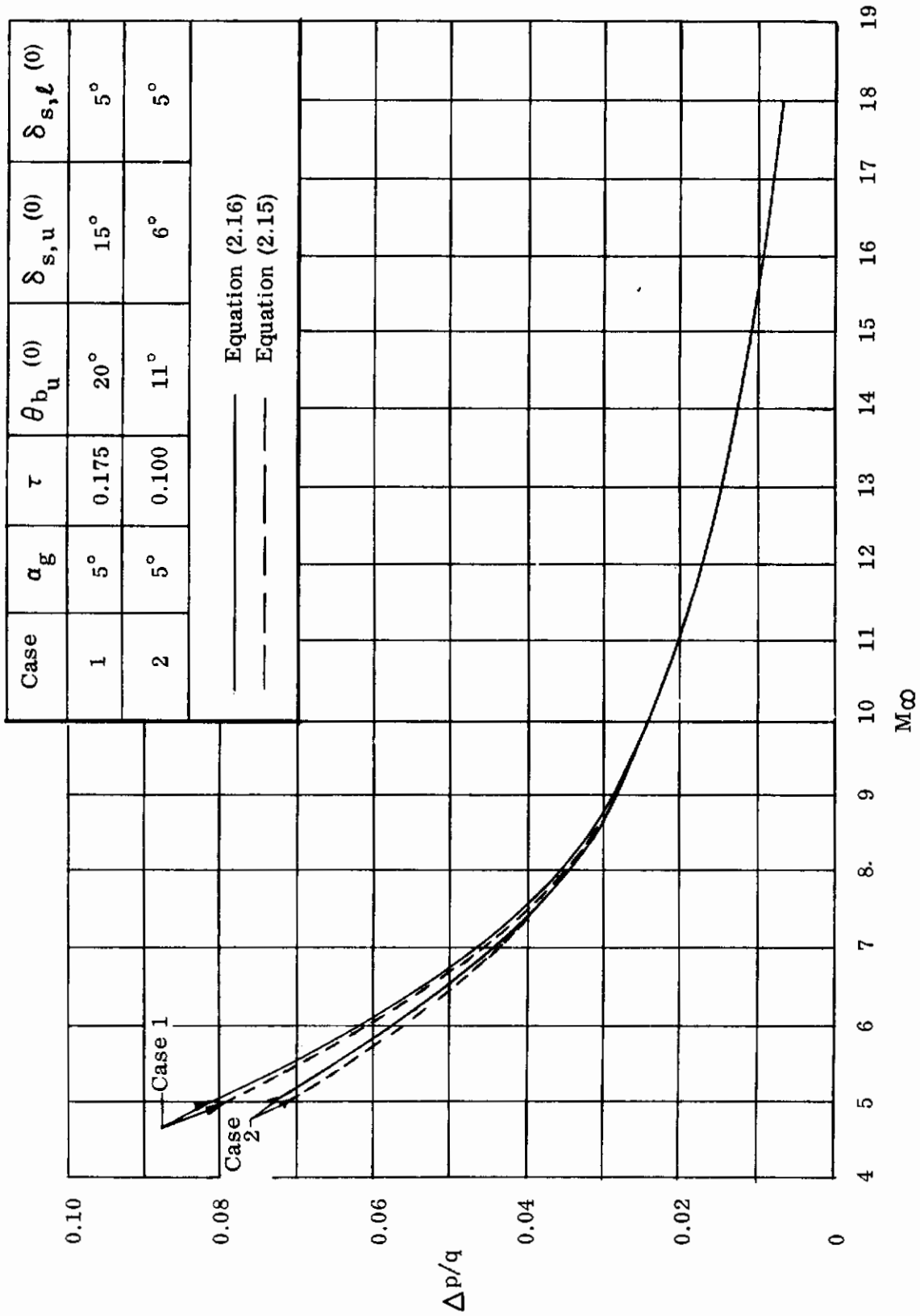Equation (2.16)
Equation (2.15)

Figure 2.7. Lifting Pressure Ratio of Half Diamond Airfoil

$$0.5 \leq \frac{x}{c} \leq 1.0$$

16

$$\left(\frac{M_s}{M_\infty}\right)^2 = \left[\frac{1}{\left(\frac{\gamma+1}{4}\right)K_s^2 P_s + 1}\right]\left[\frac{\left(\frac{\gamma+1}{4}\right)K_s^2 P_s + 1}{\frac{\gamma}{2}K_s^2 P_s + 1}\right] \qquad (2.18)$$

Linnell had listed $\left(\frac{\gamma-1}{4}\right)$ in the denominator of the first term as $\left(\frac{\gamma+1}{4}\right)$. The accuracy of (Equation (2.18) is easily verified by substitution of Equation (2.2) into Equation (2.16).

2.2.1   Region of Validity of Linnell's Method

The region of validity of Linnell's pressure prediction method is based on both mathematical and physical approximations. These approximations arise in the derivation of the shock and expansion pressure ratio expressions. In the development of tangent-wedge theory, which predicts the shock pressures, the only physical assumption made is with respect to the flow deflection and shock wave angles. In Reference 9 it is stated that $\tan \delta_s \approx \delta_s$ which yields the approximation $0 \le \delta_s \le 15°$. No approximation is made with respect to the Mach number and it can only be assumed that tangent-wedge theory holds for $M_\infty \ge 3$. The region of validity of tangent-wedge theory in terms of the hypersonic similarity parameter $K_s = M_\infty \delta_s$, is

$$K_s \ge 0 \qquad (2.19)$$

In the development of the expansion pressure ratio relationship for hypersonic speeds the physical assumption is made that the free stream Mach number is large such that $M_s \gg 1$. This being true then the following approximations can be stated

$$\sqrt{M_s^2 - 1} \approx M_s \text{ and } \sqrt{M_e^2 - 1} \approx M_e \qquad (2.20)$$

In addition, a mathematical approximation is made in the derivation of the expansion wave turning angle ν. The formulation of a mathematical expression for ν depends upon the series representation of the arc tangent functions in the equation for ν. In the present case, only the first two terms of the infinite series representation of the arc tangent functions are used. This approximation limits the size of the expansion flow deflection angle δ_e from a mathematical point of view, physically δ_e,

17

can be of any magnitude. The Mach number limitations expressed by Equation (2.20) result in the restriction

$$M_\infty \geq 5.0 \tag{2.21}$$

Another limitation arises from the expansion pressure ratio expression, namely Equation (2.3). As previously mentioned Equation (2.3) can be used only for the condition

$$\left(\frac{\gamma - 1}{2} \right)\left(\frac{M_s}{M_\infty} \right) \quad K_e \leq 1 \tag{2.22}$$

Physically, the expansion pressure cannot have a value below zero; Equation (2.22) insures this. For $\gamma = 1.40$ Equation (2.22) becomes

$$K_e \leq 5 \left(\frac{M_\infty}{M_s} \right) \tag{2.23}$$

The Mach number ratio is greater than or equal to one so that the lower limit would be

$$K_e \leq 5.0 \tag{2.24}$$

In the shock case $K_s \geq 0$ and in the expansion case $K_e \leq 5.0$. Since these cases are used in combination in Linnell's method the maximum permissible value of the similarity parameter would be $K_\delta \leq 5.0$. In summary it can be stated that for the

Shock case only $\qquad K_s > 0 \, , \, M_\infty \geq 3.0$

Expansion case only $\qquad K_e \leq 5, \, M_\infty \geq 5.0$ $\qquad (2.25)$

Shock-Expansion Case $\qquad K_\delta \leq 5, \, M_\infty \geq 5.0$
(Linnell's Method)

The last of Equation (2.25) may be rewritten in terms of the hypersonic similarity parameter K as

$$K\theta \leq 5.0 \tag{2.26}$$

Note that no restrictions have been placed upon K.

2.2.2   Discussion of Linnell's Exact and Approximate Methods

In the discussion of Equations (2.5) to (2.7) mention was made of the difficulty an aeroelastician would have in applying Equation (2.5) to a flexible airfoil since the unknown equilibrium angle of attack at the leading edge of the airfoil, α (0), is needed in order to compute C_p. One means of overcoming this difficulty is to assign a known value to α (0) which fixes the shock flow deflection angles and portions of the expansion flow deflection angles. In addition the Mach number ratios are known since they depend upon these flow deflection angles. With these known quantities a static aeroelastic analysis could proceed unheeded, however, the question naturally arises as to what quantity or value should be assigned to α (0). Since a static aeroelastic analysis is begun by choosing a value for α_g (and other inputs such as M_∞ and altitude) the logical choice would be to set α (0) = α_g. This approach would seem to be entirely feasible as long as α_s (0)/ α_g $\ll$ 1 . The approach described above will be called Linnell's "approximate" method. The use of Equation (2.5) "per se", that is, the application of this equation using α (0) rather than α_g will be called Linnell's "exact" method. Two examples will be shown in which a static aeroelastic solution is performed by use of both the "exact" and "approximate" methods.* The first example treats the classical simple cantilevered beam while the second treats a square cantilevered wing. Geometric and structural input data for these examples are given in Reference 5, Appendix A.1.0 and Reference 6, respectively.

The two basic interaction equations for these examples are

$$\{\, \alpha \,\} = \{\, \alpha_g \,\} + \{\, \alpha_s \,\} \tag{2.27}$$

and

$$\{\, \alpha_s \,\} = q \left[\delta_{\alpha z} \right] \left[R \right] \left\{ \frac{\Delta p}{q} \right\} \tag{2.28}$$

---

* For the reader unfamiliar with the subject of Static Aeroelasticity References 5, 6, and 12 should be consulted.

where $\{\alpha_s\}$ is a column matrix of local structural slopes

$\{\frac{\Delta p}{q}\}$ is a column matrix of local lifting pressures

$\{\alpha\}$ is a column matrix of local equilibrium angles of attack.

$[\delta_{\alpha Z}]$ is a square matrix of structural slope influence coefficients

$\lfloor R \rfloor$ is a diagonal matrix of reference point areas

Equations (2.27) and (2.28) are used in conjunction with Equation (2.14) to effect a solution for the equilibrium angles of attack by use of an iteration scheme.

Results of the static aeroelastic analyses are presented in terms of equilibrium angles and pressures in Tables 2.1 and 2.2. Study of Table 2.1 shows that good agreement between the methods is obtained for the three cases considered. It appears, however, that larger differences exist between the lifting pressures than between the equilibrium angles of attack when the exact and approximate methods are compared. The general trend in the results shown in Table 2.1 are unaffected by the change in K_{δ_s} the hypersonic similarity parameter based on M_∞ and $\delta_{s\ell}$. Results for the cantilevered wing are given in Table 2.2 and show excellent agreement between Linnell's exact and approximate methods thereby further establishing the validity and use of the approximate method for static aeroelastic analysis.

It is concluded from these studies that Linnell's approximate method can be successfully used for determining hypersonic static aeroelastic solutions. In order to use this method the aeroelastician replaces $\alpha(0)$ by α_g in Equations (2.11), (2.12) and (2.14) thereby eliminating an unknown parameter. It is emphasized, however, that if the $\alpha_s(x)$ distribution were known then $\alpha(0)$ would be known and the exact method could readily be used. Such an approach is used in Section 4.0 where theoretical and experimental pressure coefficients are compared. In that section, $\alpha_s(x)$ is replaced by the known local twist and camber angles.

2.2.3 Derivation and Presentation of Lifting Pressure Functions

Lifting pressure functions using Equations (2.11) to (2.14) have been derived for the ten airfoils shown in Table 2.3. Results are given in Tables

TABLE 2.1

RESULTS OF FIRST ILLUSTRATIVE EXAMPLE

Input Data: $M_\infty = 10$, $\theta_{b_u}(0) = 2.86°$, q = 10 psf, $\tau = 0.10$

$\alpha_g = 1.50°$, $0.762 \leq |K_{\delta_s}| \leq 0.878$

Ref. Pt.	$\{\alpha\}$ Exact.	Approx.	$\{\frac{\Delta p}{q}\}$ Exact.	Approx.
1	0.0268	0.0268	0.0183	0.0188
2	0.0339	0.0340	0.0235	0.0239
3	0.0378	0.0380	0.0266	0.0269

$\alpha_g = 2.75°$, $0.980 \leq |K_{\delta_s}| \leq 1.20$

Ref. Pt.	Exact.	Approx.	Exact.	Approx.
1	0.0492	0.0492	0.0341	0.0348
2	0.0626	0.0630	0.0444	0.0456
3	0.0700	0.0707	0.0504	0.0519

$\alpha_g = 4.0°$, $1.80 \leq |K_{\delta_s}| \leq 2.21$

Ref. Pt.	Exact.	Approx.	Exact.	Approx.
1	0.0713	0.0713	0.0442	0.0436
2	0.0879	0.0879	0.0554	0.0553
3	0.0970	0.0971	0.0622	0.0624

TABLE 2.2

RESULTS OF SECOND ILLUSTRATIVE EXAMPLE

Input Data: $M_\infty = 10$, $\theta_{b_\ell}(0) = -2.866°$, $\theta_{b_u}(0) = 0°$, $\tau = 0.0250$

q = 10 psf, $\alpha_g = 1.5°$

Ref. Pt.	Exact. $\{\alpha\}$	Approx.	Exact. $\{\frac{\Delta p}{q}\}$	Approx.
1	0.0260	0.0260	0.0281	0.0281
2	0.0271	0.0271	0.0103	0.0108
3	0.0273	0.0272	0.0288	0.0288
4	0.0285	0.0285	0.0108	0.0110
5	0.0283	0.0282	0.0295	0.0294
6	0.0290	0.0289	0.0292	0.0299
7	0.0293	0.0293	0.0112	0.0117
8	0.0294	0.0293	0.0112	0.0117

2.4 and 2.6. Either the exact or approximate method may be used to compute lifting pressures from these equations. A typical derivation of a lifting pressure function is shown below. Consider the single parabolic airfoil whose geometric properties are given in Table 2.3. In accordance with Equation (2.14) the following flow deflection angles are written:

For $\quad 0 \leq \bar{a}(0) \leq 4 \qquad\qquad \bar{a}(0) \geq 4$

$$\theta_{s,u}(0) = 4 - \bar{a}(0) \qquad\qquad \theta_{s,u}(0) = 0$$

$$\theta_{s,\ell}(0) = \bar{a}(0) \qquad\qquad \theta_{s,\ell}(0) = \bar{a}(0) \qquad\qquad (2.29)$$

$$\theta_{e,u}(\xi) = 8\xi + \bar{a}(\xi) - \bar{a}(0) \qquad \theta_{e,u}(\xi) = \bar{a}(\xi) - 4(1 - 2\xi)$$

$$\theta_{e,\ell}(\xi) = \bar{a}(0) - \bar{a}(\xi) \qquad\qquad \theta_{e,\ell}(\xi) = \bar{a}(0) - \bar{a}(\xi)$$

Substitution of Equations (2.29) into Equation (2.14) yields

For $\quad 0 \leq \bar{a}(0) \leq 4$

$$\frac{\Delta p/q}{\tau^2} = \left[\frac{2}{\gamma K^2} + \left(\frac{\gamma+1}{2}\right)\bar{a}(0)^2 + \sqrt{\left(\frac{\gamma+1}{2}\right)^2 \bar{a}(0)^4 + \frac{4}{K^2}\bar{a}(0)^2} \right] X$$

$$\left[1 - \left(\frac{\gamma-1}{2}\right)\left(\frac{M_s}{M_\infty}\right)_\ell K(\bar{a}(0) - \bar{a}(\xi)) \right]^{\frac{2\gamma}{\gamma-1}} \qquad\qquad (2.30)$$

$$- \left[\frac{2}{\gamma K^2} + \left(\frac{\gamma+1}{2}\right)(4 - \bar{a}(0))^2 + \sqrt{\left(\frac{\gamma+1}{2}\right)^2 (4 - \bar{a}(0))^4 + \frac{4}{K^2}(4 - \bar{a}(0))^2} \right] X$$

$$\left[1 - \left(\frac{\gamma-1}{2}\right)\left(\frac{M_s}{M_\infty}\right)_u K(8\xi + \bar{a}(\xi) - \bar{a}(0)) \right]^{\frac{2\gamma}{\gamma-1}}$$

For $\qquad \bar{a}\,(0) \geq 4$

$$\frac{\Delta p/q}{\tau^2} = \left[\frac{2}{\gamma\,K^2} + \left(\frac{\gamma+1}{2}\right) \bar{a}\,(0)^2 + \sqrt{\left(\frac{\gamma+1}{2}\right)^2 \bar{a}\,(0)^4 + \frac{4}{K^2}\,\bar{a}\,(0)^2} \right] X$$

$$\left[1 - \left(\frac{\gamma-1}{2}\right)\left(\frac{M_s}{M_\infty}\right)_\ell K\,(\bar{a}\,(0) - \bar{a}\,(\xi)) \right]^{\frac{2\gamma}{\gamma-1}} \qquad (2.31)$$

$$- \frac{2}{\gamma\,K^2}\left[1 - \left(\frac{\gamma-1}{2}\right)K\,(\bar{a}\,(\xi) - 4\,(1 - 2\,\xi)) \right]^{\frac{2\gamma}{\gamma-1}}$$

Equations (2.30) and (2.31) may be rewritten in the notation of Table 2.4 as

$$\frac{\Delta p/q}{\tau^2} = (r_0 + r_1)\,e_1 - (r_0 + r_7)\,e_{11} \quad \text{valid for} \qquad \begin{array}{l} 0 \leq \bar{a}\,(0) \leq 4, \quad (2.32) \\ 0 \leq \xi \leq 1 \end{array}$$

$$\frac{\Delta p/q}{\tau^2} = (r_0 + r_1)\,e_1 - r_0\,e_{12} \qquad \text{valid for} \qquad \begin{array}{l} \bar{a}\,(0) \geq 4 \qquad (2.33) \\ 0 \leq \xi \leq 1 \end{array}$$

From study of Equation (2.14) and Tables 2.4 to 2.6 it is seen that the lifting pressure expression is a complex nonlinear function of the equilibrium angle of attack as well as other pertinent parameters. For purposes of efficient static aeroelastic analyses the present formulation of the lifting pressure functions is not satisfactory. It is best to express aerodynamic inputs for such analyses in the form of aerodynamic influence coefficient matrices. The next section of this report describes the formulation of Linnell's method in influence coefficient form. Means for obtaining these influence coefficients are described and are presented graphically in Volume 2 of this report.
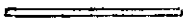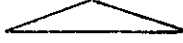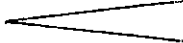
23

TABLE 2.3

SUMMARY OF AIRFOIL SHAPES AND SLOPES
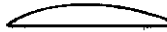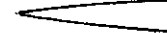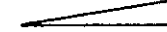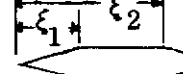
Airfoil	Equation	Slope	
Flat Plate	$\eta_u = \eta_\ell = 0$	$g_u = g_\ell = 0$	$, 0 \leq \xi \leq 1$
Half Diamond	$\eta_u = 2\xi$	$g_u = 2$	$, 0 \leq \xi \leq 0.50$
	$\eta_u = 2(1-\xi)$	$g_u = -2$	$, 0.50 \leq \xi \leq 1$
	$\eta_\ell = 0$	$g_\ell = 0$	$, 0 \leq \xi \leq 1$
Double Wedge	$\eta_u = 0.50\xi$	$g_u = 0.50$	$, 0 \leq \xi \leq 1$
	$\eta_\ell = -\eta_u$	$g_\ell = -g_u$	
Diamond	$\eta_u = \xi$	$g_u = 1$	$, 0 \leq \xi \leq 0.50$
	$\eta_u = 1-\xi$	$g_u = -1$	$, 0.5 \leq \xi \leq 1$
	$\eta_\ell = -\xi$	$g_\ell = -1$	$, 0 \leq \xi \leq 0.50$
	$\eta_\ell = \xi -1$	$g_\ell = 1$	$, 0.5 \leq \xi \leq 1$
Single Parabolic	$\eta_u = 4\xi(1-\xi)$	$g_u = 4(1-2\xi)$	$, 0 \leq \xi \leq 1$
	$\eta_\ell = 0$	$g_\ell = 0$	$, 0 \leq \xi \leq 1$
Double Parabolic - Blunt T.E.	$\eta_u = 0.50\xi(2-\xi)$	$g_u = 1-\xi$	$, 0 \leq \xi \leq 1$
	$\eta_\ell = -\eta_u$	$g_\ell = -g_u$	
Single Wedge	$\eta_u = \xi$	$g_u = 1$	$, 0 \leq \xi \leq 1$
	$\eta_\ell = 0$	$g_\ell = 0$	$, 0 \leq \xi \leq 1$
Single Parabolic Blunt T.E.	$\eta_u = \xi(2-\xi)$	$g_u = 2(1-\xi)$	$, 0 \leq \xi \leq 1$
	$\eta_\ell = 0$	$g_\ell = 0$	$, 0 \leq \xi \leq 1$
Single Wedge - Plate	$\eta_u = \xi / \xi_1$	$g_u = 1/\xi_1$	$, 0 \leq \xi \leq \xi_1$
	$\eta_u = 1$	$g_u = 0$	$, \xi_1 \leq \xi \leq 1$
	$\eta_\ell = 0$	$g_\ell = 0$	$, 0 \leq \xi \leq 1$
Modified Double Wedge	$\eta_u = 0.50\, \xi / \xi_1$	$g_u = \dfrac{0.50}{\xi_1}$	$, 0 \leq \xi \leq \xi_1$
	$\eta_u = 0.50$	$g_u = 0$	$, \xi_1 \leq \xi \leq \xi_2$
	$\eta_u = 0.50\left(\dfrac{1-\xi}{\xi_1}\right)$	$g_u = -\dfrac{0.50}{\xi_1}$	$, \xi_2 \leq \xi \leq 1$
$\xi_2 = 1 - \xi_1$	$\eta_\ell = -\eta_u$	$g_\ell = -g_u$	

24

TABLE 2.4

SUMMARY OF LIFTING PRESSURE FUNCTIONS

Airfoil	$\Delta p/q \big/ \tau^2$ for $0 \leq \bar{a}(0) \leq g_u(0)$	Valid
Flat Plate	$\bar{r}_0 \bar{e}_{20} - (\bar{r}_0 + \bar{r}_1) \bar{e}_2$ for $a(0) \leq 0$, $\tau = 0$	$0 \leq \xi \leq 1.0$
Half-Diamond	$(r_0 + r_1) e_1 - (r_0 + r_2) e_2$ $(r_0 + r_1) e_1 - (r_0 + r_2) e_3$	$0 \leq \xi \leq 0.50$ $0.50 \leq \xi \leq 1$
Double Wedge	$(r_0 + r_3) e_1 - (r_0 + r_4) e_2$	$0 \leq \xi \leq 1$
Diamond	$(r_0 + r_5) e_1 - (r_0 + r_6) e_2$ $(r_0 + r_5) e_7 - (r_0 + r_6) e_8$	$0 \leq \xi \leq 0.50$ $0.50 \leq \xi \leq 1$
Single Parabolic	$(r_0 + r_1) e_1 - (r_0 + r_7) e_{11}$	$0 \leq \xi \leq 1$
Double Parabolic Blunt T.E.	$(r_0 + r_5) e_{13} - (r_0 + r_6) e_{14}$	$0 \leq \xi \leq 1$
Single Wedge	$(r_0 + r_1) e_1 - (r_0 + r_6) e_2$	$0 \leq \xi \leq 1$
Single Parabolic Blunt T.E.	$(r_0 + r_1) e_1 - (r_0 + r_2) e_{16}$	$0 \leq \xi \leq 1$
Single Wedge – Plate	$(r_0 + r_1) e_1 - (r_0 + r_8) e_2$ $(r_0 + r_1) e_1 - (r_0 + r_8) e_{18}$	$0 \leq \xi \leq \xi_1$ $\xi_1 \leq \xi \leq 1$
Modified Double Wedge	$(r_0 + r_9) e_1 - (r_0 + r_{10}) e_2$ $(r_0 + r_9) e_{21} - (r_0 + r_{10}) e_{22}$ $(r_0 + r_9) e_{23} - (r_0 + r_{10}) e_{24}$	$0 \leq \xi \leq \xi_1$ $\xi_1 \leq \xi \leq \xi_2$ $\xi_2 \leq \xi \leq 1$

25

TABLE 2.4 (CONT)

Airfoil	$\Delta p/q \big/ \tau^2$ for $\bar{a}(0) \le g_u(0)$	Valid
Flat Plate	$(\bar{r}_0 + \bar{r}_1)\, \bar{e}_1 - \bar{r}_0\, \bar{\bar{e}}_{20}$ for $a(0) \ge 0$, $\tau = 0$	$0 \le \xi \le 1.0$
Half-Diamond	$(r_0 + r_1)\, e_1 - r_0 e_4$	$0 \le \xi \le 0.50$
	$(r_0 + r_1)\, e_1 - r_0 e_5$	$0.5 \le \xi \le 1$
Double-Wedge	$(r_0 + r_3)\, e_1 - r_0 e_6$	$0 \le \xi \le 1$
Diamond	$(r_0 + r_5)\, e_1 - r_0 e_9$	$0 \le \xi \le 0.50$
	$(r_0 + r_5)\, e_7 - r_0 e_{10}$	$0.50 \le \xi \le 1$
Single Parabolic	$(r_0 + r_1)\, e_1 - r_0 e_{12}$	$0 \le \xi \le 1$
Double Parabolic Blunt T.E.	$(r_0 + r_5)\, e_{13} - r_0 e_{15}$	$0 \le \xi \le 1$
Single Wedge	$(r_0 + r_1)\, e_1 - r_0 e_9$	$0 \le \xi \le 1$
Single Parabolic Blunt T.E.	$(r_0 + r_1)\, e_1 - r_0 e_{17}$	$0 \le \xi \le 1$
Single Wedge-Plate	$(r_0 + r_1)\, e_1 - r_0 e_{19}$	$0 \le \xi \le \xi_1$
	$(r_0 + r_1)\, e_1 - r_0 e_{20}$	$\xi_1 \le \xi \le 1$
Modified Double Wedge	$(r_0 + r_9)\, e_1 - r_0 e_{25}$	$0 \le \xi \le \xi_1$
	$(r_0 + r_9)\, e_{21} - r_0 e_{20}$	$\xi_1 \le \xi \le \xi_2$
	$(r_0 + r_9)\, e_{23} - r_0 e_{26}$	$\xi_2 \le \xi \le 1$

TABLE 2.5

TABULATION OF r FUNCTIONS

$$r_0 = \frac{2}{\gamma K^2}, \quad \bar{r}_0 = \frac{2}{\gamma M_\infty^2}$$

$$r_1 = \left(\frac{\gamma+1}{2}\right)\bar{a}(0)^2 + \sqrt{\left(\frac{\gamma+1}{2}\right)^2 \bar{a}(0)^4 + \frac{4}{K^2}\bar{a}(0)^2}$$

$$\bar{r}_1 = \left(\frac{\gamma+1}{2}\right)a(0)^2 + \sqrt{\left(\frac{\gamma+1}{2}\right)^2 a(0)^4 + \frac{4}{M_\infty^2 a(0)^2}}$$

$$r_2 = \left(\frac{\gamma+1}{2}\right)[2-\bar{a}(0)]^2 + \sqrt{\left(\frac{\gamma+1}{2}\right)^2 [2-\bar{a}(0)]^4 + \frac{4}{K^2}[2-\bar{a}(0)]^2}$$

$$r_3 = \left(\frac{\gamma+1}{2}\right)[\bar{a}(0)+0.50]^2 + \sqrt{\left(\frac{\gamma+1}{2}\right)^2 [\bar{a}(0)+0.50]^4 + \frac{4}{K^2}[\bar{a}(0)+0.50]^2}$$

$$r_4 = \left(\frac{\gamma+1}{2}\right)[0.50-a(0)]^2 + \sqrt{\left(\frac{\gamma+1}{2}\right)^2 [0.50-\bar{a}(0)]^4 + \frac{4}{K^2}[0.50-\bar{a}(0)]^2}$$

$$r_5 = \left(\frac{\gamma+1}{2}\right)[\bar{a}(0)+1]^2 + \sqrt{\left(\frac{\gamma+1}{2}\right)^2 [\bar{a}(0)+1]^4 + \frac{4}{K^2}[\bar{a}(0)+1]^2}$$

$$r_6 = \left(\frac{\gamma+1}{2}\right)[1-\bar{a}(0)]^2 + \sqrt{\left(\frac{\gamma+1}{2}\right)^2 [1-\bar{a}(0)]^4 + \frac{4}{K^2}[1-\bar{a}(0)]^2}$$

$$r_7 = \left(\frac{\gamma+1}{2}\right)[4-\bar{a}(0)]^2 + \sqrt{\left(\frac{\gamma+1}{2}\right)^2 [4-\bar{a}(0)]^4 + \frac{4}{K^2}[4-\bar{a}(0)]^2}$$

$$r_8 = \left(\frac{\gamma+1}{2}\right)\left[\frac{1}{\xi_1}-\bar{a}(0)\right]^2 + \sqrt{\left(\frac{\gamma+1}{2}\right)^2 \left[\frac{1}{\xi_1}-\bar{a}(0)\right]^4 + \frac{4}{K^2}\left[\frac{1}{\xi_1}-\bar{a}(0)\right]^2}$$

$$r_9 = \left(\frac{\gamma+1}{2}\right)\left[\bar{a}(0)+\frac{0.50}{\xi_1}\right]^2 + \sqrt{\left(\frac{\gamma+1}{2}\right)^2 \left[\bar{a}(0)+\frac{0.50}{\xi_1}\right]^4 + \frac{4}{K^2}\left[\bar{a}(0)+\frac{0.50}{\xi_1}\right]^2}$$

$$r_{10} = \left(\frac{\gamma+1}{2}\right)\left[\frac{0.50}{\xi_1}-\bar{a}(0)\right]^2 + \sqrt{\left(\frac{\gamma+1}{2}\right)^2 \left[\frac{0.50}{\xi_1}-\bar{a}(0)\right]^4 + \frac{4}{K^2}\left[\frac{0.50}{\xi_1}-\bar{a}(0)\right]^2}$$

TABLE 2.6

TABULATION OF e FUNCTIONS

$$e_1 = \left[1 - \frac{\gamma-1}{2}\left(\frac{M_s}{M_\infty}\right)_\ell K\left[\bar{a}(0) - \bar{a}(\xi)\right]\right]^{\frac{2\gamma}{\gamma-1}}$$

$$\bar{e}_1 = \left[1 - \left(\frac{\gamma-1}{2}\right)\left(M_s/M_\infty\right)_\ell M_\infty\left(a(0) - a(\xi)\right)\right]^{\frac{2\gamma}{\gamma-1}}$$

$$e_2 = \left[1 + \left(\frac{\gamma-1}{2}\right)\left(\frac{M_s}{M_\infty}\right)_u K\left[\bar{a}(0) - \bar{a}(\xi)\right]\right]^{\frac{2\gamma}{\gamma-1}}$$

$$e_3 = \left[1 + \left(\frac{\gamma-1}{2}\right)\left(\frac{M_s}{M_\infty}\right)_u K\left[4 + \bar{a}(\xi) - \bar{a}(0)\right]\right]^{\frac{2\gamma}{\gamma-1}}$$

$$e_4 = \left[1 - \left(\frac{\gamma-1}{2}\right) K\left[\bar{a}(\xi) - 2\right]\right]^{\frac{2\gamma}{\gamma-1}}$$

$$e_5 = \left[1 - \left(\frac{\gamma-1}{2}\right) K\left[\bar{a}(\xi) + 2\right]\right]^{\frac{2\gamma}{\gamma+1}}$$

$$e_6 = \left[1 - \left(\frac{\gamma-1}{2}\right) K\left[\bar{a}(\xi) - 0.50\right]\right]^{\frac{2\gamma}{\gamma+1}}$$

$$e_7 = \left[1 - \left(\frac{\gamma-1}{2}\right)\left(\frac{M_s}{M_\infty}\right)_\ell K\left[2 + \bar{a}(0) - \bar{a}(\xi)\right]\right]^{\frac{2\gamma}{\gamma+1}}$$

$$e_8 = \left[1 - \left(\frac{\gamma-1}{2}\right)\left(\frac{M_s}{M_\infty}\right)_u K\left[2 + \bar{a}(\xi) - \bar{a}(0)\right]\right]^{\frac{2\gamma}{\gamma+1}}$$

$$e_9 = \left[1 - \left(\frac{\gamma-1}{2}\right) K\left[\bar{a}(\xi) - 1\right]\right]^{\frac{2\gamma}{\gamma+1}}$$

$$e_{10} = \left[1 - \left(\frac{\gamma-1}{2}\right) K\left[\bar{a}(\xi) + 1\right]\right]^{\frac{2\gamma}{\gamma+1}}$$

$$\bar{e}_2 = \left[1 - \left(\frac{\gamma-1}{2}\right)\left(\frac{M_s}{M_\infty}\right)_u M_\infty\left[\bar{a}(0) - \bar{a}(\xi)\right]\right]^{\frac{2\gamma}{\gamma-1}}$$

28

TABLE 2.6 (CONT)

$$e_{11} = \left[1 - \left(\frac{\gamma-1}{2} \right) \left(\frac{M_s}{M_\infty} \right)_u K \left[8\xi + \overline{a}(\xi) - \overline{a}(0) \right] \right]^{\frac{2\gamma}{\gamma+1}}$$

$$e_{12} = \left[1 - \left(\frac{\gamma-1}{2} \right) K \left[\overline{a}(\xi) - 4(1-2\xi) \right] \right]^{\frac{2\gamma}{\gamma+1}}$$

$$e_{13} = \left[1 - \left(\frac{\gamma-1}{2} \right) \left(\frac{M_s}{M_\infty} \right)_\ell K \left[\xi - \overline{a}(\xi) + \overline{a}(0) \right] \right]^{\frac{2\gamma}{\gamma-1}}$$

$$e_{14} = \left[1 - \left(\frac{\gamma-1}{2} \right) \left(\frac{M_s}{M_\infty} \right)_u K \left[\xi + \overline{a}(\xi) - \overline{a}(0) \right] \right]^{\frac{2\gamma}{\gamma-1}}$$

$$e_{15} = \left[1 - \left(\frac{\gamma-1}{2} \right) K \left[\overline{a}(\xi) + \xi - 1 \right] \right]^{\frac{2\gamma}{\gamma-1}}$$

$$e_{16} = \left[1 - \left(\frac{\gamma-1}{2} \right) \left(\frac{M_s}{M_\infty} \right)_u K \left[2\xi + \overline{a}(\xi) - \overline{a}(0) \right] \right]^{\frac{2\gamma}{\gamma-1}}$$

$$e_{17} = \left[1 - \left(\frac{\gamma-1}{2} \right) K \left[\overline{a}(\xi) - 2(1-\xi) \right] \right]^{\frac{2\gamma}{\gamma-1}}$$

$$e_{18} = \left[1 - \left(\frac{\gamma-1}{2} \right) \left(\frac{M_s}{M_\infty} \right)_u K \left[\frac{1}{\xi_1} + \overline{a}(\xi) - \overline{a}(0) \right] \right]^{\frac{2\gamma}{\gamma-1}}$$

$$e_{19} = \left[1 - \left(\frac{\gamma-1}{2} \right) K \left[\overline{a}(\xi) - \frac{1}{\xi_1} \right] \right]^{\frac{2\gamma}{\gamma-1}}$$

$$e_{20} = \left[1 - \left(\frac{\gamma-1}{2} \right) K \overline{a}(\xi) \right]^{\frac{2\gamma}{\gamma-1}}, \quad \overline{e}_{20} = \left[1 + \left(\frac{\gamma-1}{2} \right) M_\infty \ a(0) \right]^7$$

$$\overline{\overline{e}}_{20} = \left[1 - \left(\frac{\gamma-1}{2} \right) M_\infty \ a(\xi) \right]^{\frac{2\gamma}{\gamma-1}}$$

$$e_{21} = \left[1 - \left(\frac{\gamma-1}{2} \right) \left(\frac{M_s}{M_\infty} \right)_\ell K \left[\frac{0.50}{\xi_1} + \overline{a}(0) - \overline{a}(\xi) \right] \right]^{\frac{2\gamma}{\gamma-1}}$$

TABLE 2.6 (CONT)

$$e_{22} = \left[1 - \left(\frac{\gamma-1}{2} \right) \left(\frac{M_s}{M_\infty} \right)_u K \left[\frac{0.50}{\xi_1} + \bar{a}(\xi) - \bar{a}(0) \right] \right]^{\frac{2\gamma}{\gamma-1}}$$

$$e_{23} = \left[1 - \left(\frac{\gamma-1}{2} \right) \left(\frac{M_s}{M_\infty} \right)_\ell K \left[\frac{1}{\xi_1} + \bar{a}(0) - \bar{a}(\xi) \right] \right]^{\frac{2\gamma}{\gamma-1}}$$

$$e_{24} = \left[1 - \left(\frac{\gamma-1}{2} \right) \left(\frac{M_s}{M_\infty} \right)_u K \left[\frac{1}{\xi_1} + \bar{a}(\xi) - \bar{a}(0) \right] \right]^{\frac{2\gamma}{\gamma-1}}$$

$$e_{25} = \left[1 - \left(\frac{\gamma-1}{2} \right) K \left[\bar{a}(\xi) - \frac{0.50}{\xi_1} \right] \right]^{\frac{2\gamma}{\gamma-1}}$$

$$e_{26} = \left[1 - \left(\frac{\gamma-1}{2} \right) K \left[\bar{a}(\xi) + \frac{0.50}{\xi_1} \right] \right]^{\frac{2\gamma}{\gamma-1}}$$

SECTION 3.0

FORMULATION AND PRESENTATION OF AERODYNAMIC INFLUENCE COEFFICIENTS

3.1   GENERAL

The concept of an aerodynamic influence coefficient, or an array of such coefficients, which is called an aerodynamic influence coefficient matrix, has been previously discussed in References 13 and 14. The matrix relationship between angle of attack and lifting pressure can be written as

$$\left\{ \frac{\Delta p}{q} \right\} = \left[Q \right] \left\{ \alpha \right\} \tag{3.1}$$

where $\left[Q \right]$ is defined as an aerodynamic influence coefficient matrix. Equation (3.1) is based on the assumption that the relationship between pressure and angle of attack is linear. This is generally considered to be true in the supersonic speed regime; it is not, however, necessarily true at hypersonic speeds. This then leads to a new definition of aerodynamic influence coefficients for the higher speeds.

Consider the half span swept wing shown in Figure 3.1 with the hypersonic "pressure loadings" $\left(\frac{\Delta p}{q} \right)_i$ and $\left(\frac{\Delta p}{q} \right)_j$ at points i and j, respectively. It had
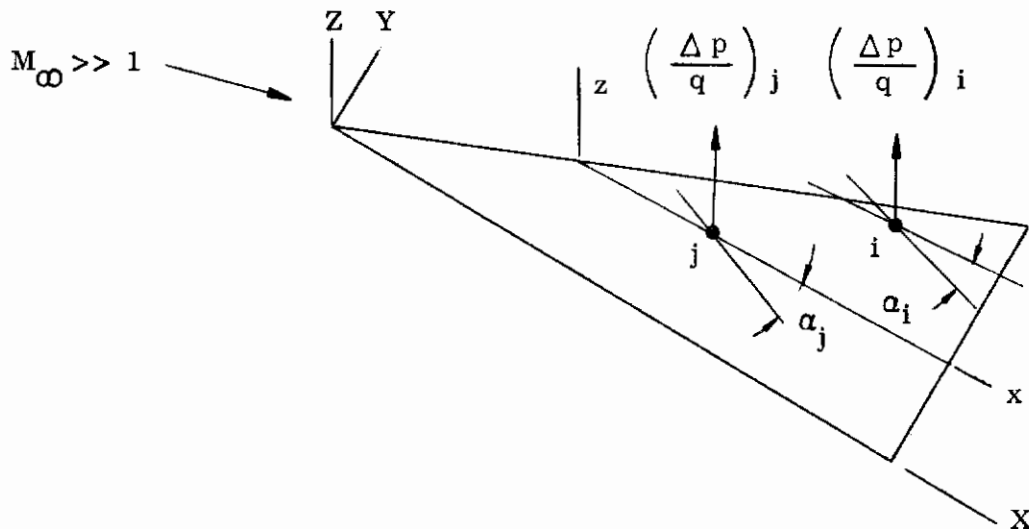

Figure 3.1. Aid in Defining an Influence Coefficient

been demonstrated in Reference 1 that the lifting pressure at point i is a function of the angle of attack at point i only and not at j as well. Likewise, $(\frac{\Delta p}{q})_j$ is a function of α_j only. In this manner the "influence" of α_j upon $(\frac{\Delta p}{q})_i$ does not exist. Also, α_i does not affect $(\frac{\Delta p}{q})_j$. Therefore, one needs only to consider the basic relationship between $(\frac{\Delta p}{q})_i$ and α_i in order to determine the desired aerodynamic influence coefficients. Aerodynamic influence coefficients in the hypersonic case are defined as "those quantities which relate the aerodynamic load (or pressure) at a particular point to the angle of attack at the same point and only that point". This definition yields diagonal influence coefficient matrices since the off-diagonal elements are zero. The off-diagonal elements relate the aerodynamic load to the angle of attack at other points than the one in question and this relation or influence does not exist in the hypersonic case. The above definition can best be shown mathematically. In general, it may be written that

$$\left(\frac{\Delta p}{q}\right)_i = F_i (\alpha_i) \tag{3.2}$$

According to Reference 1 typical forms of Equation (3.2) are

$$F_i (\alpha_i) = q_{0_i} + q_{2_i} \alpha_i^2 \tag{3.3}$$

$$F_i (\alpha_i) = q_{1_i} \alpha_i + q_{3_i} \alpha_i^3 \tag{3.4}$$

The quantities q_{0_i}, q_{1_i} etc. are aerodynamic influence coefficients as previously defined. The subscripts 0, 1, 2 . . . . n are equal to the powers of α_i which they premultiply. The influence coefficients are functions of the parameters ξ_i, τ, M_∞, γ, and airfoil shape. Equations (3.2) to (3.4) can be readily put into matrix form. This is highly desirable since it preserves existing static aeroelastic notation and matrix techniques previously developed in supersonic and hypersonic aeroelasticity studies.

32

3.2 COMPUTATION OF AERODYNAMIC INFLUENCE COEFFICIENTS

Since Linnell's pressure relationships are complex functions of the equilibrium angle of attack it would be advantageous to reformulate this method to yield relations such as Equations (3.2) to (3.4). This can be accomplished by computing lifting pressure values using Linnell's method and then fitting a polynomial to these values. The coefficients of the polynomial are the desired influence coefficients in accordance with the above definition. In addition, this representation satisfies two objectives, namely (1) derives an explicit relationship between lifting pressure and angle of attack and (2) derives a set of input compatible with the nonlinear static aeroelasticity FORTRAN program of Reference 6.

Curve fitting studies demonstrated that a third degree polynomial (cubic) provided the best "fit" to the lifting pressure values. Thus, aerodynamic influence coefficients were computed for the ten airfoil shapes listed in Table 2.3 using an IBM 7090 electronic digital computer. The lifting pressure relationship given by Equations (2.11) to (2.14) was programmed in FORTRAN language. Included in the program was a least-squares curve fitting procedure which fit a cubic equation to the lifting pressure values computed by use of Equation (2.13). Program input data consisted of the geometry of the airfoil and the parameters ξ_1, $\bar{\alpha}(0)$, $\bar{\alpha}(\xi)$ and K.

The general computational procedure used is as follows:

(1) Select airfoil geometry.

(2) Select ξ_1, ξ, $\bar{\alpha}(0)$ and K values. (Note that $\bar{\alpha}(0)$ is not taken to be $\bar{\alpha}_g$ at this point. For purposes of aeroelastic analyses the aeroelastician can then choose $\bar{\alpha}(0) \equiv \bar{\alpha}_g$ when formulating the $\lfloor Q_n \rfloor$ matrices.)

(3) Input Items (1) and (2) into the FORTRAN program.

(4) Compute $\left(\frac{\Delta p}{q}\right)_i / \tau^2$ versus $\bar{\alpha}(\xi)$ for known sets of $\bar{\alpha}(0)$, K for $\xi_{,1}$, and ξ values.

(5) Use least-squares curve fitting subroutine to fit a cubic equation to the data of step (4).

(6) Print out the coefficients of the cubic and the standard deviation σ of the curve fit.

Typical results of Steps (1) through (5) are shown in Figure 3.2. Standard engineering plots are used to present the aerodynamic influence coefficients as a function of K and α (0) for each section listed in Table 2.3.

Numerical values of the parameters $\bar{\alpha}(\xi)$, $\bar{\alpha}(0)$, and K were chosen to best describe flight conditions, airfoil geometry and static aeroelastic deformations that would be encountered by a practicing aeroelastician. The maximum airfoil thickness ratio is assumed to be equal to 0.20. With this assumption, numerical ranges of the parameters can be defined. For the moderate hypersonic speed range K will then have the values $0 \le K \le 3$. By definition $\bar{\alpha}(0) \equiv \bar{\alpha}_g$ when Linnell's approximate method is used. $\bar{\alpha}_g$ is a function of the thickness ratio τ and the maximum value of α_g permissible. Figure 3.3 displays $\bar{\alpha}(0)$ versus τ for various values of α_g. From this figure it can be seen that an upper limit of $\bar{\alpha}(0) = 5.0$ is more than sufficient to cover the τ range when a maximum value of $\alpha_g = 15°$ is chosen. The range of the parameter $\bar{\alpha}(\xi)$ depends upon the structural slopes $\alpha_s(\xi)$ and thickness ratio. Figure 3.4 shows $\bar{\alpha}(\xi)$ as a function of τ, $\alpha_s(\xi)$ and α_g assuming various multiples of α_g for $\alpha_s(\xi)$. It is seen from this figure that an $\bar{\alpha}_{max}(\xi) = 3.0$ and $\alpha_s = 0.50 \, \alpha_g$ is sufficient.

The SHARE subroutine described in Reference 15 was used to fit a third degree polynomial to the lifting pressure points obtained from the FORTRAN program. This subroutine fits polynomials of order one through seven to N given points by the method of least squares. The standard deviation σ was used as a measure of how well this subroutine fit the pressure points. A $\sigma \le 1.0$ was considered acceptable for a satisfactory curve fit. It was found that the value of σ could be grossly affected by the numerical values of $\bar{\alpha}(\xi)$ chosen in the computing process. Results of curve fitting studies dictated that the lower portion of the interval $0 \le \bar{\alpha}(\xi) \le 3.0$ be heavily populated with pressure points in order to keep $\sigma \le 1.0$.

34

Half – Diamond

$\bar{a}\,(0) = 5.0$

$K = 1.50$

Least – Squares Fit –

$$\triangle \frac{\Delta p/q}{\tau^2} = -14.22 + 22.50\,\bar{a} - 8.15\,\bar{a}^2 + 1.50\,\bar{a}^3, \sigma = 0.120$$

$$\triangle \frac{\Delta p/q}{\tau^2} = \quad 2.59 + 2.22\,\bar{a} + 0.489\,\bar{a}^2 + 0.252\,\bar{a}^3, \sigma = 0.0102$$

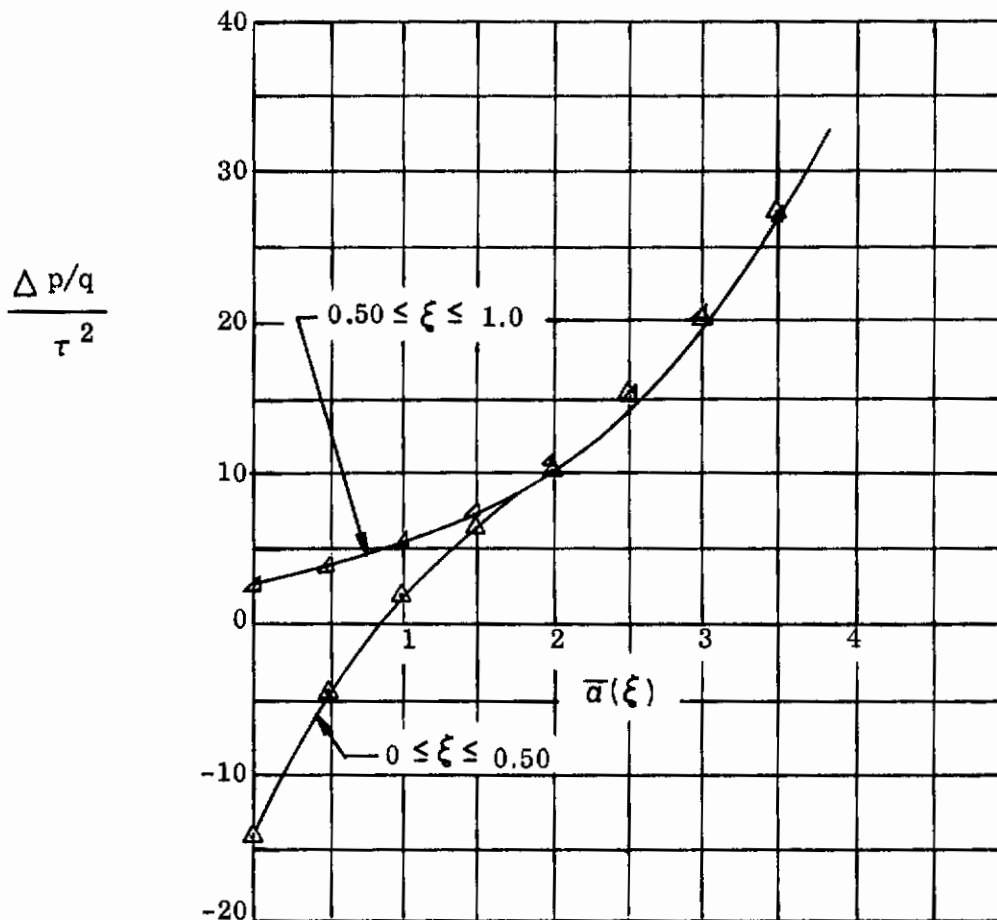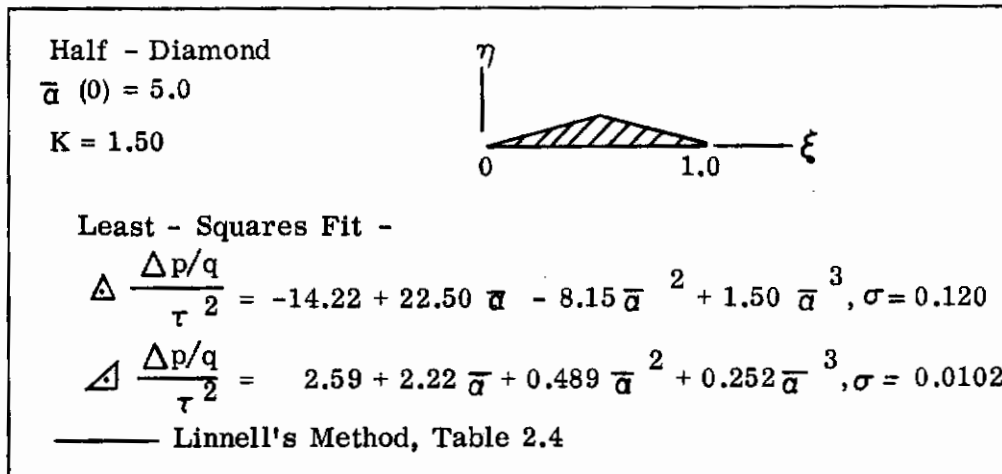———— Linnell's Method, Table 2.4

Figure 3.2. Typical Lifting Pressure Curve Fit
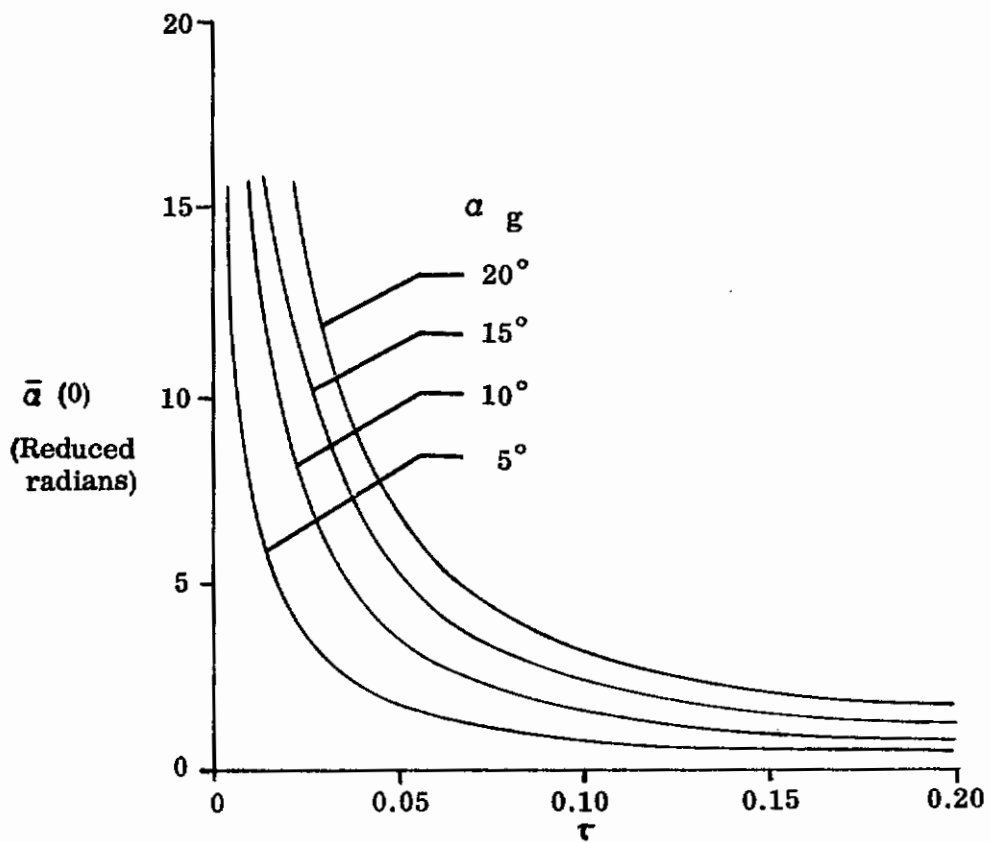
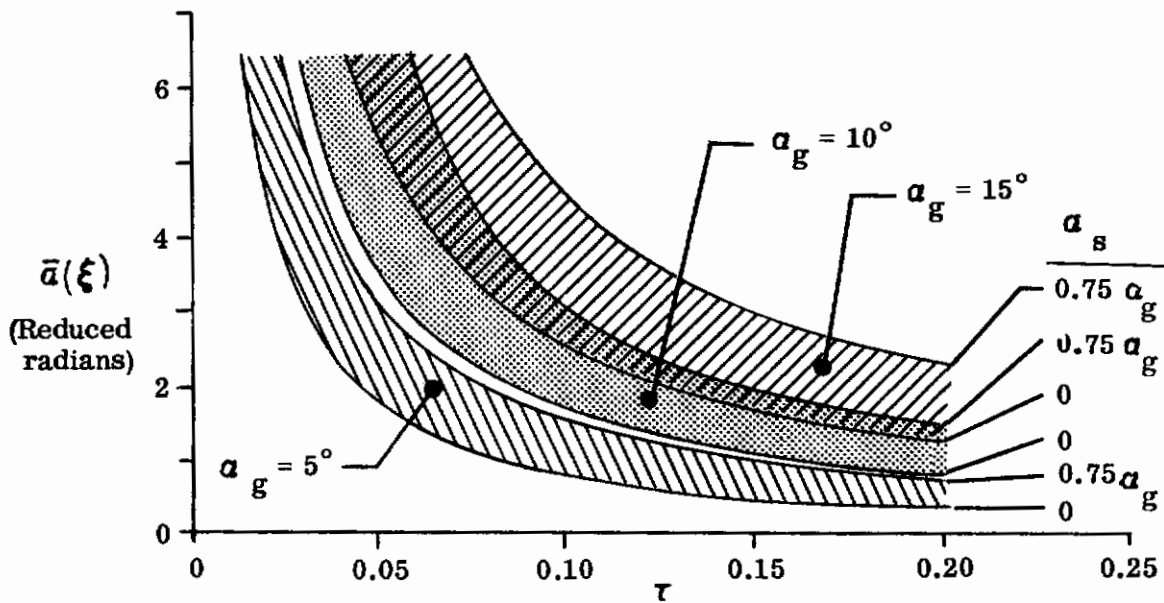Figure 3.3. Parameter $\bar{a}$ (0) versus τ

Figure 3.4. Parameter $\bar{a}$ (ξ) versus τ

36

3.3   ILLUSTRATIVE EXAMPLE

The method for determining aerodynamic influence coefficients for a slender sharp nose airfoil is presented. Consider a rectangular wing with cross-sectional and flow properties as shown in Table 3.1. Using this information and Figures 5 to 14 in Volume 2, the coefficients given in the center portion of Table 3.1 are obtained. Experimental values for this wing are available in Reference 16. Using the coefficients in Table 3.1 yields the comparisons shown in the lower portion of the table. Although theoretical predictions are somewhat higher than test values, the comparisons shown in Table 3.1 are considered to be satisfactory when the inherent inaccuracies in the test data are taken into account. It is noted that the theoretical lifting pressures obtained by using Dorrance's method, Reference 1, agree within 10% of those obtained using Linnell's method.

TABLE 3.1

INPUT DATA AND RESULTS FOR ILLUSTRATIVE EXAMPLE

		Input Data		
		Half Diamond Section		
		$M_\infty = 6.86, \quad c = 4$ inches		
		$2b = 4$ inches, $\quad \tau = 0.050$		
		$\alpha_g = 0°, 6°$		

Aerodynamic Influence Coefficients

$\bar{\alpha}(o) = 0, \quad K = 0.343$

ξ_i	q_{0_i}	q_{1_i}	q_{2_i}	q_{3_i}
0.050	-0.0426	0.905	-0.950	6.60
0.315	-0.0426	0.905	-0.950	6.60
0.685	0.0218	0.390	0.500	4.00
0.950	0.0218	0.390	0.500	4.00

$\bar{\alpha}(o) = 2.09, \quad K = 0.343$

ξ_i	q_{0_i}	q_{1_i}	q_{2_i}	q_{3_i}
0.050	-0.0435	0.920	-1.05	6.00
0.315	-0.0435	0.920	-1.05	6.00
0.685	0.0208	0.390	0.550	3.80
0.950	0.0208	0.390	0.550	3.80

Theory to Test Comparisons

$$\left\{ \frac{\Delta p}{q} \right\}$$

ξ_i	$\left\{ \alpha_g \right\} = \left\{ 0° \right\}$		$\left\{ \alpha_g \right\} = \left\{ 6° \right\}$	
	Test	Theory	Test	Theory
0.050	-0.0404	-0.0426	0.0467	0.0506
0.315	-0.0402	-0.0426	0.0456	0.0506
0.685	-0.0153	0.0218	0.0623	0.0720
0.950	0.0199	0.0218	0.0596	0.0720

SECTION 4.0

COMPARISONS OF THEORETICAL AND EXPERIMENTAL PRESSURE DISTRIBUTIONS

4.1 GENERAL

The purpose of this chapter is to present comparisons of theoretical and experimental pressure distributions in order to evaluate Dorrance's and Linnell's pressure prediction methods as to their accuracy and range of validity when applied to warped and twisted wing geometries. Experimental data obtained on Contract AF33(616)-6846 by Grumman Aircraft Engineering Corporation for the Flight Control Laboratory, Aeronautical Systems Division was used. Results of this program are available through Reference 10.

Comparisons are graphically shown in two ways. First there is the type of presentation shown in Figure 4.3. A line of perfect agreement between theory and test and lines of ±10 percent deviation are shown. Although many features, such as chordwise and spanwise variation of the pressure coefficients, are not readily distinguishable, this method of presentation was chosen as the most feasible manner of comparing theory to test values in a reasonable number of figures. Only data points of maximum and minimum theory to test agreement have been presented. In this manner test data scatter can be shown. The second means of displaying comparisons are the use of standard engineering plots such as shown in Figure 4.4. It is noted however that only typical sets of comparisons are given in order to give the reader a better understanding of the chordwise variation of the pressure coefficient.

### 4.2 DESCRIPTION OF WING MODELS AND TEST CONDITIONS

A thorough description of the wing models, tunnel test conditions, instrumentation and run schedules is given in Reference 10. For the sake of completeness a brief review of these items are included in this report. Tests were conducted on the following wing models, sketched in Figures 4.1 and 4.2, at nominal Mach numbers of 12.0 and 19.0:

39
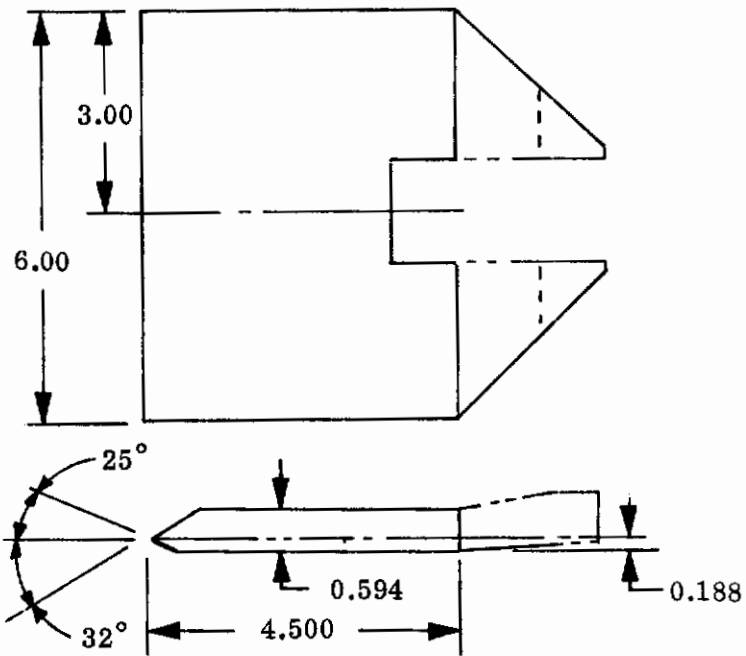
Dimensions in Inches

Figure 4.1. Sketch of Flat Rectangular Wing
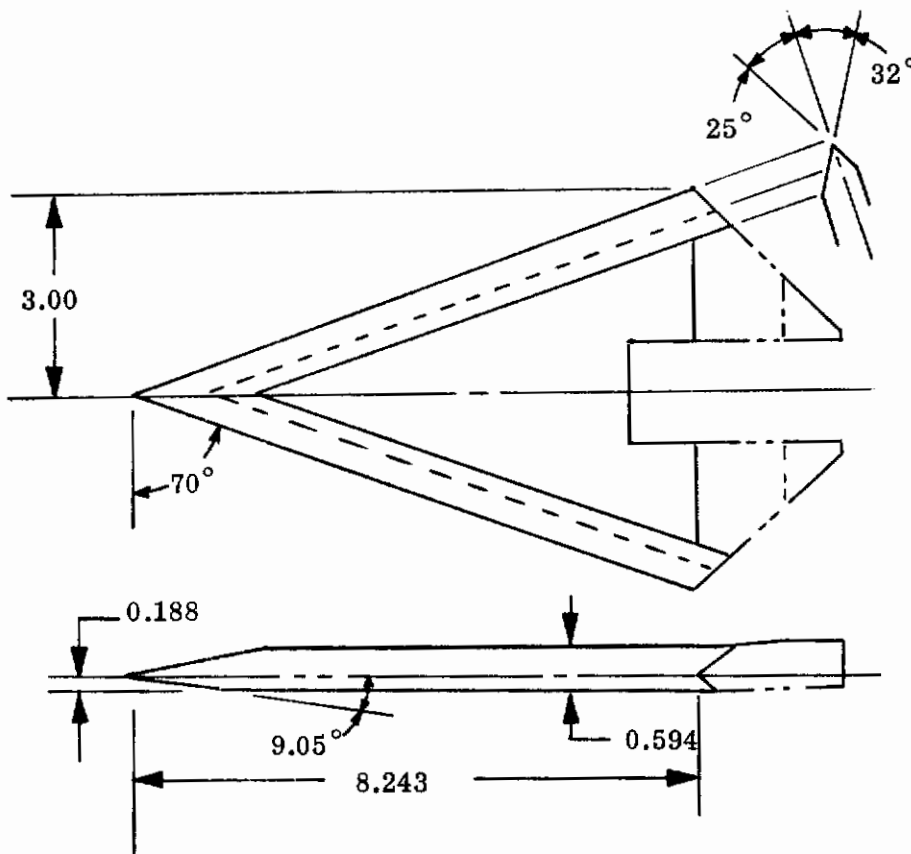
Dimensions in Inches

Figure 4.2. Sketch of Flat 70° Delta Wing

40

A.   Rectangular Planform

	Condition	Twist Distribution
1.	Flat	$\alpha_s = 0$
2.	Circular-arc camber	$\alpha_s = 5\text{-}10 \ (x/c)$
3.	Symmetrical linear twist	$\alpha_s = 5(y/b/2)$

B.   70° Delta Planform

	Condition	Twist Distribtuion
1.	Flat	$\alpha_s = 0$
2.	Circular-arc camber	$\alpha_s = 5\text{-}10 \ (x/c)$
3.	Sine-wave camber	$\alpha_s = 5 \cos 2\pi \ (x/c_{root})$

Twenty pressure transducers were located within each wing model measuring pressures on the lower surface only. During test the geometric angle of attack, α_g, was varied from 0 to 15° in steps 0°, 2°, 5°, 10° and 15°.

To use Dorrance's or Linnell's pressure prediction methods, the unknown equilibrium angle of attack distribution, Equation (2.27), must be determined. Although the test models are not "flexible", aeroelastically speaking, they can be considered to be so by taking $\left\{ \alpha_s \right\}$ to be the local spanwise twist, or local chordwise camber angle. This approach was used for both wing models. The $\left\{ \alpha \right\}$ distributions so derived are listed in Tables 4.1 and 4.2.

4.3   COMPARISONS USING DORRANCE'S METHOD

This pressure prediction method states that the local pressure coefficient is a function of the local flexible flow deflection angle at the point of interest. As stated mathematically in Reference 1, C_p for the lower surface of the model is

$$C_{p_\ell} = M_\infty^2 \ \delta \ell_f + \left(\frac{\gamma+1}{2}\right) \ \delta^2 \ell_f + \left(\frac{\gamma+1}{6}\right) M_\infty \ \delta^3 \ell_f \qquad (4.1)$$

41

TABLE 4.1

EQUILIBRIUM ANGLE OF ATTACK DISTRIBUTIONS – RECTANGULAR WING

Flat:

α_g $\frac{x}{c}$	0° α	2° α	5° α	10° α	15° α
0.050	0	0.03490	0.08725	0.17450	0.26175
0.149	↓	↓	↓	↓	↓
0.260					
0.371					
0.482					
0.593					
0.704	↓	↓	↓	↓	↓

Linear Twist:

α_g y/b/2	0° α^*	2° α	5° α	10° α	15° α
0	0	0.03490	0.08725	0.17450	0.26175
0.500	0.04363	0.07859	0.13028	0.21813	0.30538
0.917	0.07128	0.10618	0.15853	0.24518	0.33303

*The α distributions are valid at all chordwise positions at any particular spanwise position.

Circular Arc Camber:

α_g $\frac{x}{c}$	0° α	2° α	5° α	10° α	15° α
0.050	0.07853	0.11343	0.16648	0.25303	0.34028
0.149	0.06125	0.09615	0.14850	0.23575	0.32300
0.260	0.04188	0.07678	0.12913	0.21638	0.30363
0.371	0.02251	0.05745	0.10976	0.19701	0.28426
0.482	0.00314	0.03804	0.09039	0.17764	0.26489
0.593	-0.01623	0.01867	0.07102	0.15827	0.24552
0.704	-0.03560	-0.00070	0.05165	0.13894	0.22615

TABLE 4.2

EQUILIBRIUM ANGLE OF ATTACK DISTRIBUTION
70° DELTA WING

Flat:

α_g	0°	2°	5°	10°	15°
$\left(\dfrac{x}{c}\right)_{Root}$	α	α	α	α	α
0	0	0.03490	0.08725	0.17450	0.26175
0.237	↓	↓	↓	↓	↓
0.384					
0.532					
0.679					
0.827					
0.974	↓	↓	↓	↓	↓

Circular Arc Camber:

α_g	0°	2°	5°	10°	15°
$\left(\dfrac{x}{c}\right)_{Root}$	α	α	α	α	α
0	0.08725	0.12215	0.17450	0.26175	0.34900
0.237	0.04589	0.08079	0.13314	0.22039	0.30764
0.384	0.02199	0.05689	0.10924	0.19649	0.28374
0.532	-0.00558	0.02932	0.08167	0.16892	0.25592
0.679	-0.03212	0.00278	0.05513	0.14238	0.22938
0.827	-0.05706	-0.02216	0.03019	0.11744	0.20444
0.974	-0.08271	-0.04781	0.00537	0.09179	0.17904

Sine Wave Camber:

α_g	0°	2°	5°	10°	15°
$\left(\dfrac{x}{c}\right)_{Root}$	α	α	α	α	α
0	0.08725	0.12215	0.17450	0.26175	0.34900
0.237	0.00685	0.04175	0.09410	0.18135	0.26860
0.284	-0.06500	-0.03010	0.02225	0.10950	0.19675
0.532	-0.08568	-0.05078	0.00157	0.08882	0.17607
0.679	-0.04092	-0.00602	0.04633	0.13358	0.22083
0.827	0.04092	0.07582	0.12817	0.21542	0.30927
0.974	0.08603	0.12095	0.17328	0.26053	0.34778

where the flexible flow deflection angle $\delta_{\ell_f}(x)$ is defined as

$$\delta_{\ell_f}(x) = a - \theta_{b\ell}(x) \tag{4.2}$$

Substitution of Equation (4.2) into Equation (4.1) and rewriting the result in matrix form for all reference points gives the result

$$\left\{ c_{p_\ell} \right\} = \lfloor Q_o \rfloor \left\{ 1 \right\} + \lfloor Q_1 \rfloor \left\{ a \right\} + \lfloor Q_2 \rfloor \left\{ a^2 \right\} + \lfloor Q_3 \rfloor \left\{ a^3 \right\} \tag{4.3}$$

where the elements of the aerodynamic influence coefficient matrices are given by

$$q_{0_i} = -\left(\frac{\gamma+1}{6}\right) M_\infty \theta_{b\ell}^{3}(x) + \left(\frac{\gamma+1}{2}\right) \theta_{b\ell}^{2}(x) - \frac{2}{M_\infty} \theta_{b\ell}(x)$$

$$q_{1_i} = \frac{2}{M_\infty} - (\gamma + 1) \theta_{b\ell}(x) + \left(\frac{\gamma+1}{2}\right) M_\infty \theta_{b\ell}^{2}(x)$$

$$q_{2_i} = \left(\frac{\gamma+1}{2}\right) - \left(\frac{\gamma+1}{2}\right) M_\infty \theta_{b\ell}(x)$$

$$q_{3_i} = \left(\frac{\gamma+1}{6}\right) M_\infty \tag{4.4}$$

Using the geometric properties of each wing model and the values $\gamma = 1.4$ and $M_\infty = 12.6, 12.8, 18.9,$ and 19.2 yields the results shown in Table 4.3. It should be noted that in applying Dorrance's method to a swept wing the geometric properties of the swept wing in the free stream direction should be used.

Use of Equation (4.3) and the tabular inputs in Tables 4.1 and 4.2 yields the pressure coefficients shown in Figures 4.3 to 4.17. Experimental data is shown by the various symbols while theoretical data is shown by solid lines. Results for the rectangular wing will be discussed first. Figure 4.3 gives a quick comparison of Dorrance's method with test data. The majority of the predicted pressure coefficients are below test values. Figures 4.4 to 4.9 show the chordwise variation of the pressure coefficients. Note the values of the hypersonic similarity parameters $\left| K_\delta \right|$. Test data might indicate that Dorrance's method could be used for $\left| K_\delta \right| \geq 1.50$. The chordwise trends of the test pressure coefficients for the circular arc

44

TABLE 4.3

TABULATION OF AERODYNAMIC INFLUENCE COEFFICIENTS, DORRANCE'S METHOD

Rectangular Wing:	$\theta_{b\ell} = -0.4363$	$0 \leq \dfrac{x}{c} \leq 0.0892$		
	$\theta_{b\ell} = 0$	$0.0892 \leq \dfrac{x}{c} \leq 1.00$		
M_∞	12.8		19.2	
q_n	$0 \leq \dfrac{x}{c} \leq 0.0892$	$0.0892 \leq \dfrac{x}{c} \leq 1.00$	$0 \leq \dfrac{x}{c} \leq 0.0892$	$0.0892 \leq \dfrac{x}{c} \leq 1.00$
q_0	0.7218	0	0.9117	0
q_1	4.1273	0.1562	5.5371	0.1042
q_2	7.9016	1.200	11.4524	1.200
q_3	5.1200	5.120	7.680	7.680

70° Delta Wing:	$\theta_{b\ell} = -0.15811$	$0 \leq \dfrac{x}{c_{Root}} \leq 0.1434$		
	$\theta_{b\ell} = 0$	$0.1434 \leq \dfrac{x}{c_{Root}} \leq 1.00$		
M_∞	12.6		18.9	
q_n	$0 \leq \dfrac{x}{c_{Root}} \leq 0.1434$	$0.1434 \leq \dfrac{x}{c_{Root}} \leq 1.0$	$0 \leq \dfrac{x}{c_{Root}} \leq 0.1434$	$0.1434 \leq \dfrac{x}{c_{Root}} \leq 1.0$
q_0	0.0750	0	0.0766	0
q_1	0.9160	0.1587	1.0520	0.1058
q_2	3.591	1.20	4.786	1.200
q_3	5.040	5.04	7.560	7.560

cambered airfoil are predicted by Dorrance's method. However, the spanwise variation of the test pressure coefficients for the flat and circular arc cambered airfoils are not predicted by this method. Theory dictates that C_p is constant across the wing span since α depends only on x/c.

Figures 4.11 to 4.17 show comparisons for the $70°$ delta wing. As shown by Figure 4.11, theoretical values of C_p are for the most part greater than experimental values. Best results have been obtained for the sine-wave cambered wing. Trends in the experimental data are predicted by Dorrance's method. Note the good agreement between Dorrance's and Linnell's exact methods for $\left| K_\delta \right| \leq 1.00$.

4.4   COMPARISONS USING LINNELL'S METHOD

Comparisons are made using Linnell's exact and approximate methods as described in Section 2.0 of this report. Equations (2.10) and (2.12) are used to derive the pressure coefficient expression for Linnell's exact method. Linnell's approximate method is used in influence coefficient form as described in Section 3.0. It is noted that comparisons are only made for the $70°$ delta wing since Linnell's method cannot be used for the rectangular wing due to the $25°$ leading edge wedge angle on this wing. This angle and the large test Mach numbers yield small values of M_s which violates one of the approximations upon which Linnell's method is based, i.e.,

$$\sqrt{M_s^2 - 1} \approx M_s \quad \text{and} \quad \sqrt{M_e^2 - 1} \approx M_e \tag{4.5}$$

In addition to the above violation, another one is present. Since M_s and consequentially M_e are not large enough, the expression for δ_e becomes less accurate since more terms in the arc tangent series must be used to describe δ_e. What this amounts to is that large errors arise in the $E(\xi)$ terms in Equation (2.13). These approximations are discussed further in Paragraph 2.2.1 of Section 2.0.

46

4.4.1 Exact Method

In accordance with Equation (2.10) the pressure coefficient expression for the lower surface of the 70° delta wing is:

$$C_{p_\ell} = \tau^2 S_\ell (o) E_\ell (x/c) - \frac{2}{\gamma M_\infty^2}, \text{ for } \alpha \, (0) \geq 0 \qquad (4.6)$$

The flow deflection angles are determined by use of Equation (2.12). Results are shown in Table 4.4. Use of these tabular entries and Equation (4.6) with $\gamma = 1.4$, $M_\infty = 12.6$ and 18.9 yields the results shown in Figures 4.10 to 4.17.

4.4.2 Approximate Method

The curve fitting procedures described in Section 3.2 were used to generate the aerodynamic influence coefficients given in Table 4.5. However, in this instance the FORTRAN program was amended so that C_{p_ℓ} was computed rather than $\frac{\Delta p}{q}$. This was necessary since test data was obtained only on the lower surface of the models. As discussed in Section 3.0, the pressure coefficients can be stated in matrix language as:

$$\{C_{p_\ell}\} = \lfloor Q_0 \rfloor \{1\} + \lfloor Q_1 \rfloor \{\alpha\} + \lfloor Q_2 \rfloor \{\alpha^2\} + \lfloor Q_3 \rfloor \{\alpha^3\} \qquad (4.7)$$

where the matrix elements are given in Table 4.5. Using these values and the entries in Table 4.2 the pressure coefficients shown on Figures 4.12 to 4.17 are obtained.

Study of Figures 4.12 to 4.17 show poor to fair agreement of Linnell's methods with test data. Best agreement is obtained for the sine-wave cambered wing. Trends in the test data, however, are definitely being predicted by both the approximate and exact methods. Note the good agreement between the exact and approximate forms of Linnell's method. This further establishes the use of the approximate form in static aeroelastic analyses.

47

TABLE 4.4

TABULATION OF FLOW DEFLECTION ANGLES, LINNELL'S
EXACT METHOD

$\left(\dfrac{x}{c}\right)_{Root}$	$\delta_{e,\ell_f}(x/c)$		
	Flat	Circular	Sine
0	0	0	0
0.237	0.15811	0.19947	0.23851
0.384		0.22337	0.31036
0.532		0.25094	0.33104
0.679		0.27660	0.28628
0.827		0.30242	0.20444
0.974		0.32807	0.15933

$$\delta_{s,\ell_f}^{(0)}$$

α_g	$0°$	$2°$	$5°$	$10°$	$15°$
Flat	0.15811	0.19301	0.24536	0.33261	0.41986
Circular Arc	0.24536	0.28026	0.33261	0.41986	0.50711
Sine – Wave	0.24536	0.28026	0.33261	0.41986	0.50711

48

TABLE 4.5

TABULATION OF AERODYNAMIC INFLUENCE COEFFICIENTS, LINNELL'S APPROXIMATE METHOD

$M_\infty = 12.6$				
$\alpha(0) = \alpha_g$	$0°$	$2°$	$5°$	$10°$
$0 \leq \xi_i \leq 0.1434$				
q_{0_i}	0.06876	0.06542	0.0629	0.06418
q_{1_i}	0.9183	0.8298	0.7311	0.6367
q_{2_i}	3.436	3.050	2.583	2.056
q_{3_i}	19.90	15.89	11.42	7.035
$0.1434 \leq \xi_i \leq 1.00$				
q_{0_i}	0.000666	0.001458	0.00314	0.00725
q_{1_i}	0.1630	0.1616	0.1640	0.1780
q_{2_i}	0.5740	0.5980	0.6240	0.6480
q_{3_i}	7.200	6.050	4.700	3.260

$M_\infty = 18.9$				
$\alpha(0) = \alpha_g$	$0°$	$2°$	$5°$	$10°$
$0 \leq \xi_i \leq 0.1434$				
q_{0_i}	0.06384	0.05967	0.05741	0.0599
q_{1_i}	0.9816	0.8381	0.7064	0.6027
q_{2_i}	3.705	3.188	2.623	2.046
q_{3_i}	32.34	22.82	14.47	7.970
$0.1434 \leq \xi_i \leq 1.00$				
q_{0_i}	0.001157	0.002157	0.004084	0.008391
q_{1_i}	0.1255	0.1249	0.1310	0.1507
q_{2_i}	0.21625	0.3523	0.4732	0.5680
q_{3_i}	9.671	7.47	5.360	3.480

4.5   SUMMARY AND CONCLUSIONS

The purpose of making theory to test comparisons was to further establish the use, accuracy, and region of validity of Dorrance and Linnell's pressure prediction methods in operator form. Due to the fair agreement between these theoretical methods and the test data no conclusive statements can be made in regards to the accuracy and range of validity of the hypersonic aerodynamic operators associated with these methods. It should not be hastily concluded however that the aerodynamic operators are of no use since the inaccuracies in the test data must be accounted for as well as any shortcomings which exist in the theoretical methods. These same theoretical methods have been successfully applied at lower hypersonic speeds (See Reference 1). In regards to the test data, the reader should consult Reference 10 for a complete discussion of data accuracy. As stated in that reference "the widest discrepancies in the test data were obtained at reference points near the leading edge. Except for these points the average scatter of the results was within ±5 percent or less. Increased scatter was apparent at the low angles of attack ($0°$ and $2°$)." Based on the above discussion and study of Figures 4.3 to 4.17 certain observations and conclusions can be made. These are:

(1)   Chordwise trends in the test pressure coefficients can be predicted using Linnell's and/or Dorrance's methods.

(2)   Predicted pressure coefficients were generally below test values for the rectangular wing and above test values for the delta wing.

(3)   Best results were obtained for the sine-wave cambered wing.

(4)   Linnell's approximate and exact methods yield essentially the same results. The approximate method gives pressure coefficients which are somewhat lower than the exact method. These values however lie between those obtained by use of Linnell's exact and Dorrance's methods.

(5)   The theoretical methods which used aerodynamic influence coefficient matrices were easy to apply to the twisted and cambered wing models.

(6)   Test data was well organized and graphically presented so that comparisons were easy to make.

50

(7) The presence of a large leading pressure gradiant adversely affec-
ted the measured pressures. This pressure gradient was caused by
the large leading edge wedge angles (see Reference 10). Further
study indicated that the effect of the pressure gradient can be sub-
tracted out to some extent for certain twist configurations. This is
easily accomplished by forming a set of incremental pressure coeffi-
cients, defined as the difference between cambered (or twisted) wing
pressures and flat wing pressures. Figures 4.18 and 4.19 show
selected results. As seen, best results are obtained for the circular
arc cambered wings; results for the linear twist and sine wave
cambered wings are less satisfactory. In addition, the comparison
generally becomes poorer as Mach number and angle of attack are
increased. Theoretical predictions show that the pressure incre-
ment is invariant along the chord (or span) and the existing experi-
mental evidence, in certain cases, tends to bear this out. As pre-
viously observed, trends in the test data are definitely predicted.
Thus, the conclusion reached is that pressure perturbations caused
by twist or camber can be adequately predicted by the methods of
this report or those in Reference 1. This would indicate that
absence of the leading edge pressure gradient could possibly result
in closer agreement between measured and predicted pressure coef-
ficients. The phenenoma of item (8), however, may affect this con-
clusion.

(8) The theoretical methods used are developed for so-called "sharp-
nose" airfoils. Hence the wing models must be geometrically and
aerodynamically sharp otherwise the "sharp-nose" inviscid pres-
sures might well be masked by either boundary layer or blunt nose
induced effects. If these effects existed then the theoretical predic-
tions would be in error.

(9) It is definitely felt that the type of tests conducted and the twisted
and cambered models chosen were worthwhile. However, tests con-
ducted on models with smaller leading edge wedge angles and at
speeds in the range $0 \leq M_{\infty} \leq 15$ would make the application of
Linnell's and Dorrance's pressure prediction methods more feasible.
It is felt that tests should simulate, as near as possible, the physical
and mathematical approximations and idealizations pertinent to a
theoretical method in order to properly assess this method as to its
validity.
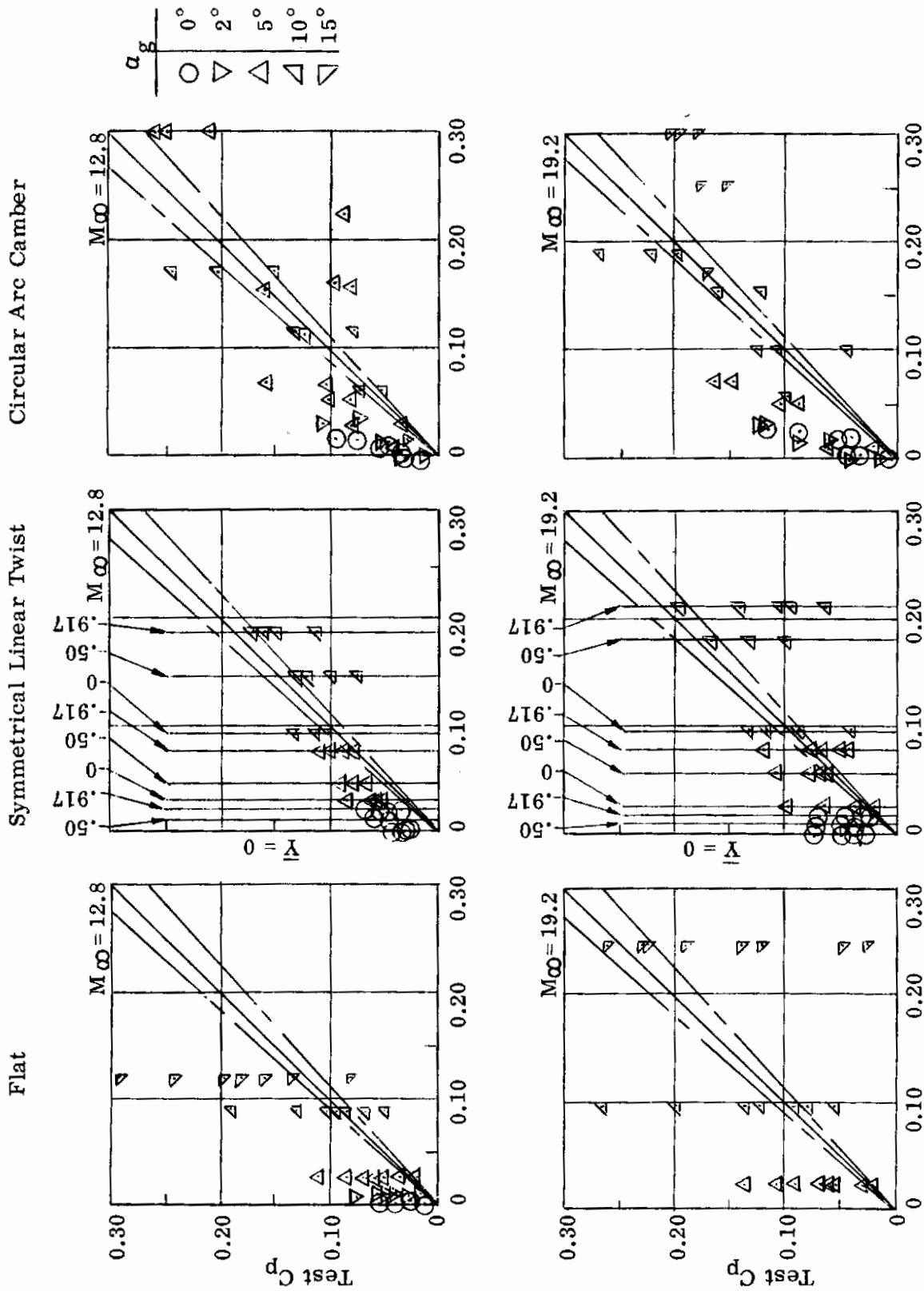
Figure 4.3 Theory to Test Comparisons – Rectangular Wing

52
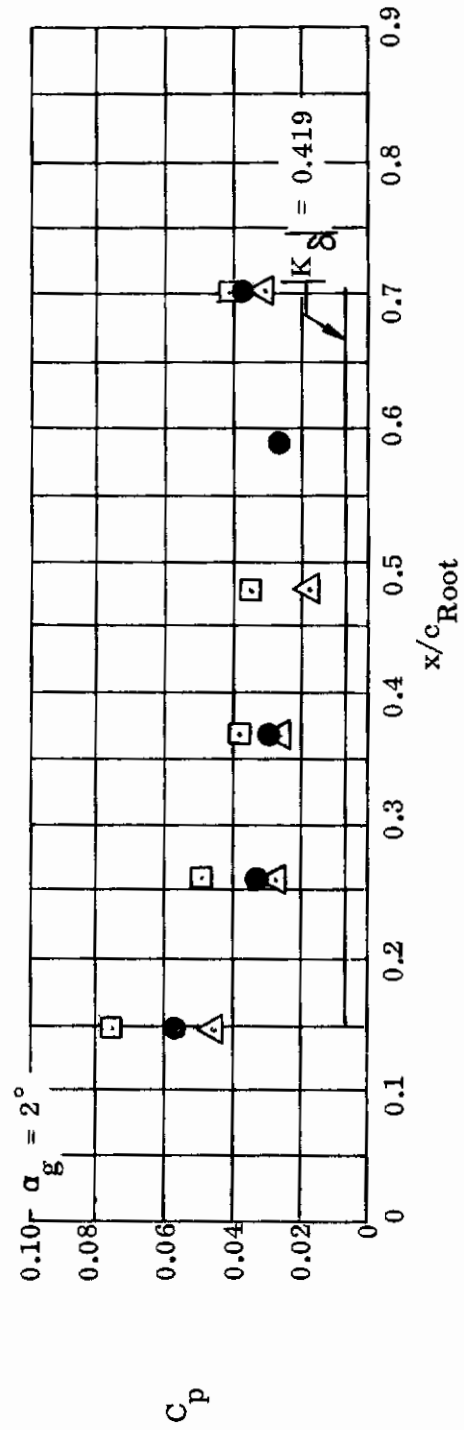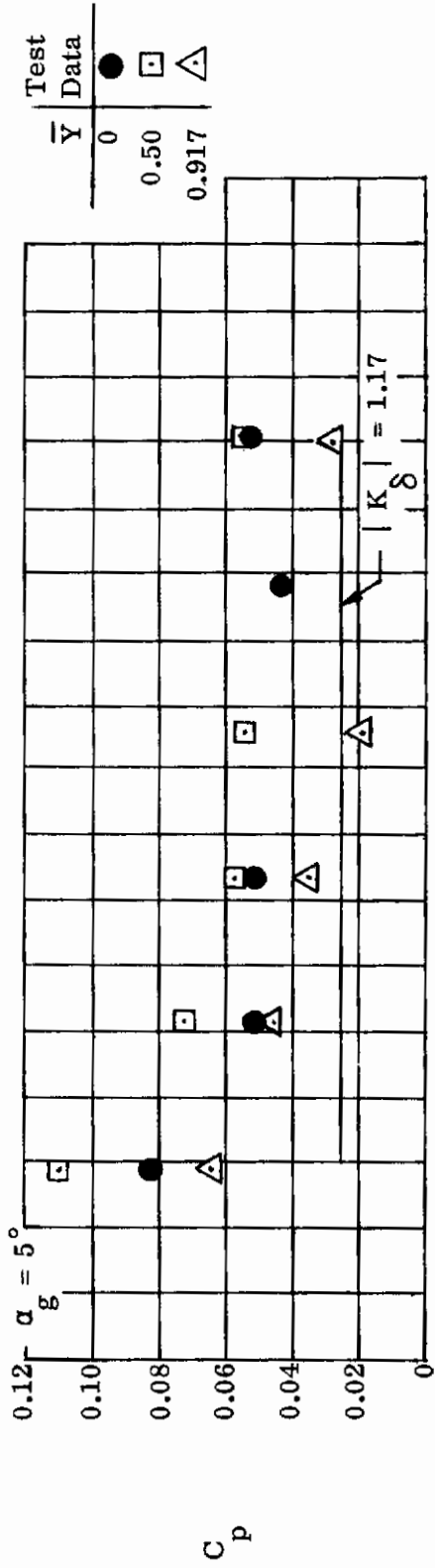
Figure 4.4. Theory to Test Comparisons Flat-Rectangular Wing M_∞ = 12.8, Dorrance's Method

53
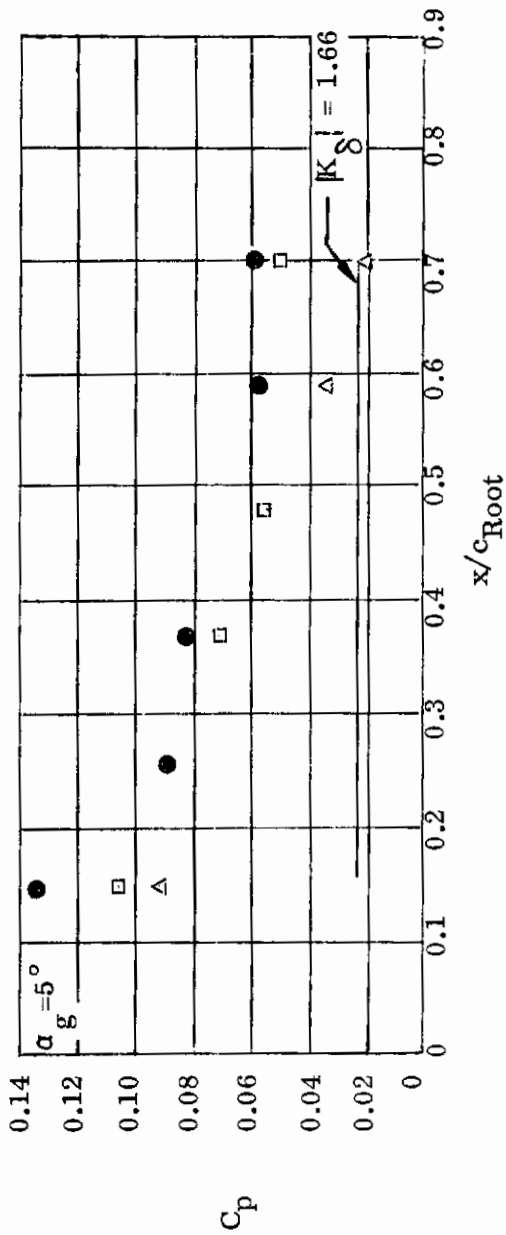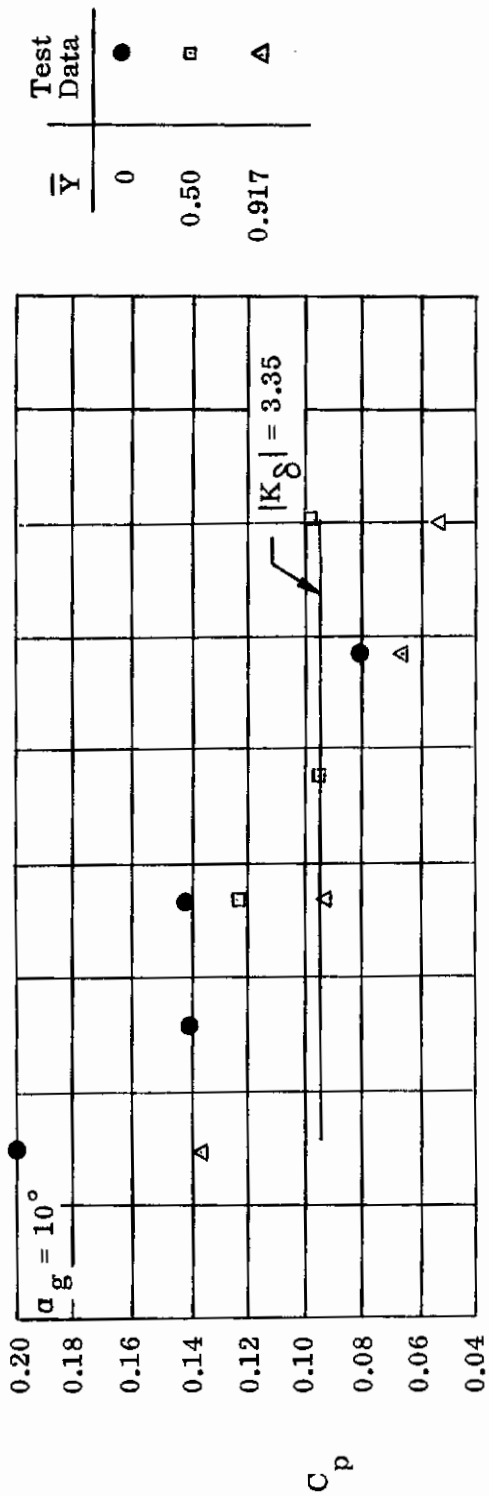
Figure 4.5.. Theory to Test Comparisons Flat – Rectangular Wing $M_\infty = 19.2$, Dorrance's Method
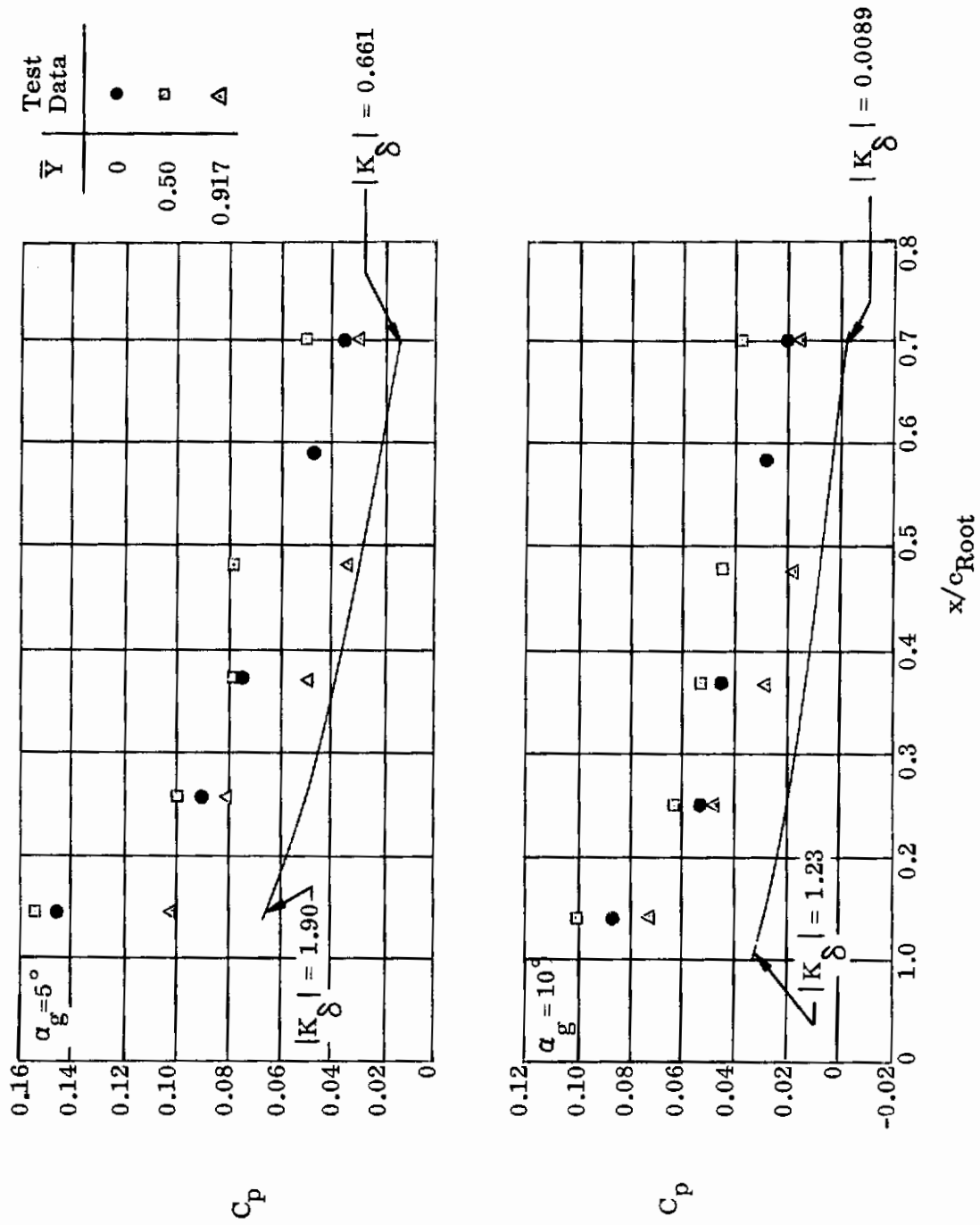
54

Figure 4.6. Theory to Test Comparisons Circular Arc Cambered Rectangular Wing M_∞ = 12.8, Dorrance's Method
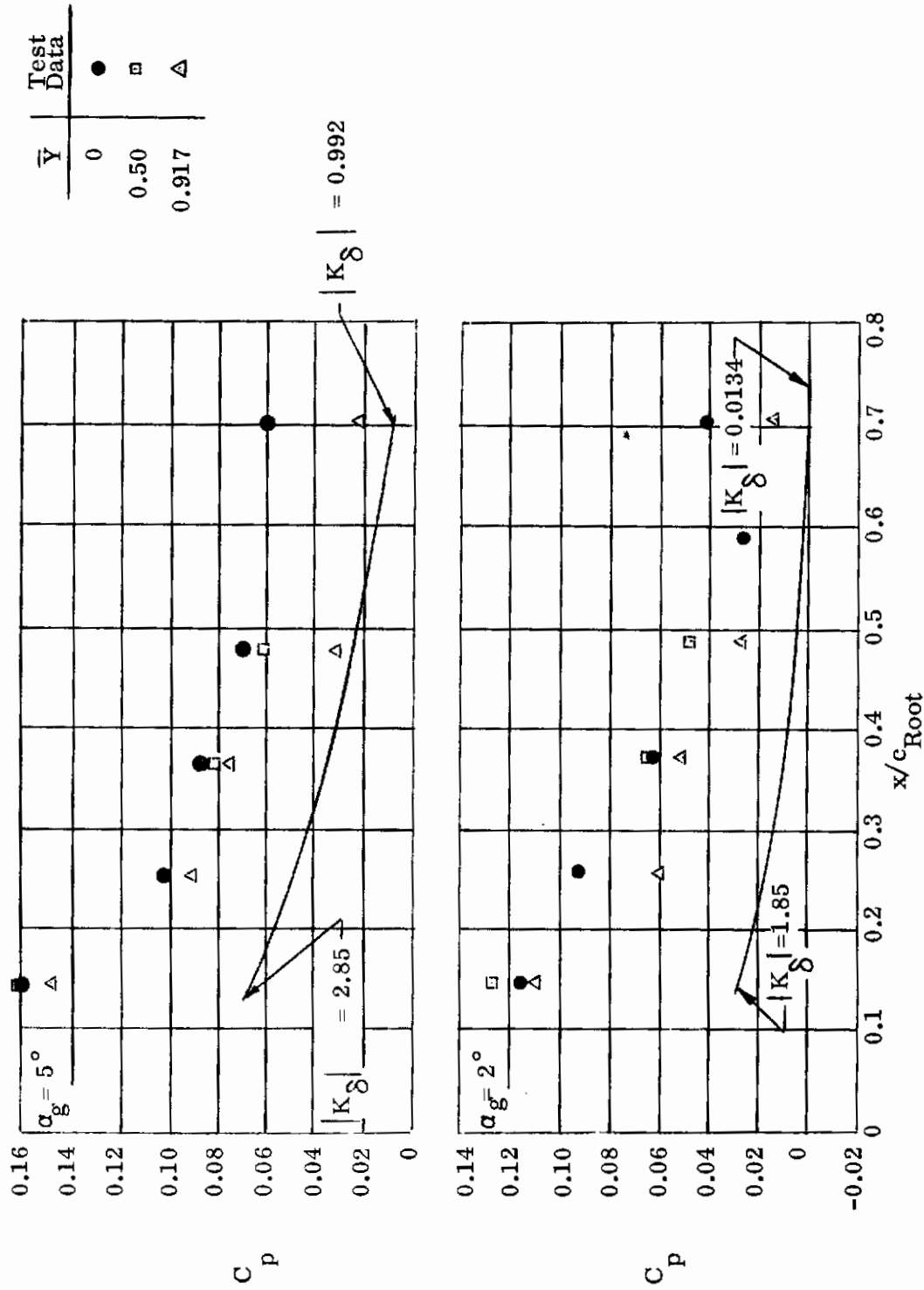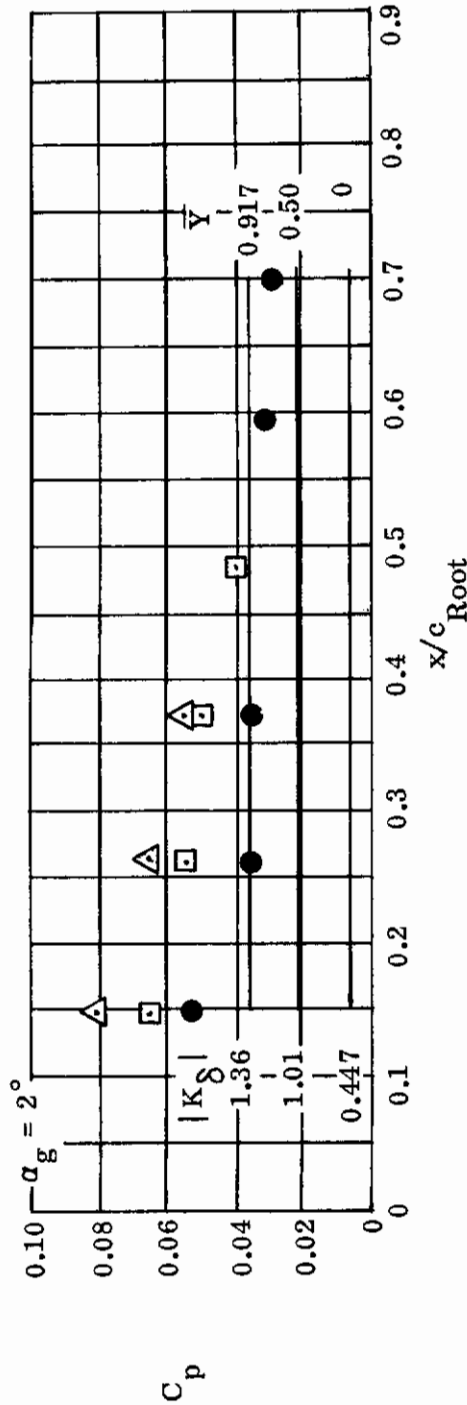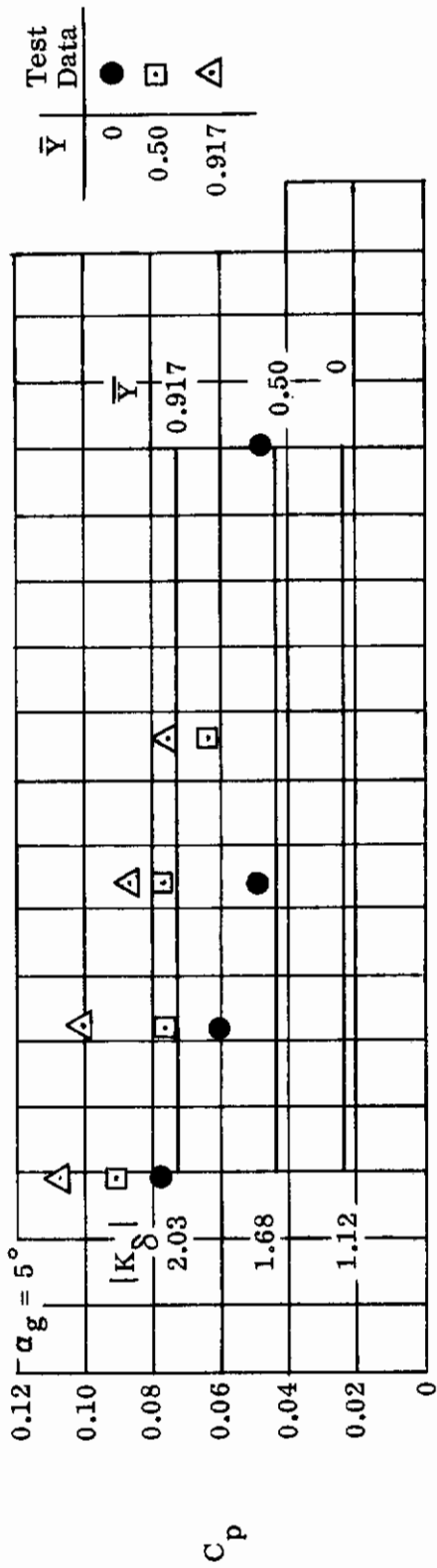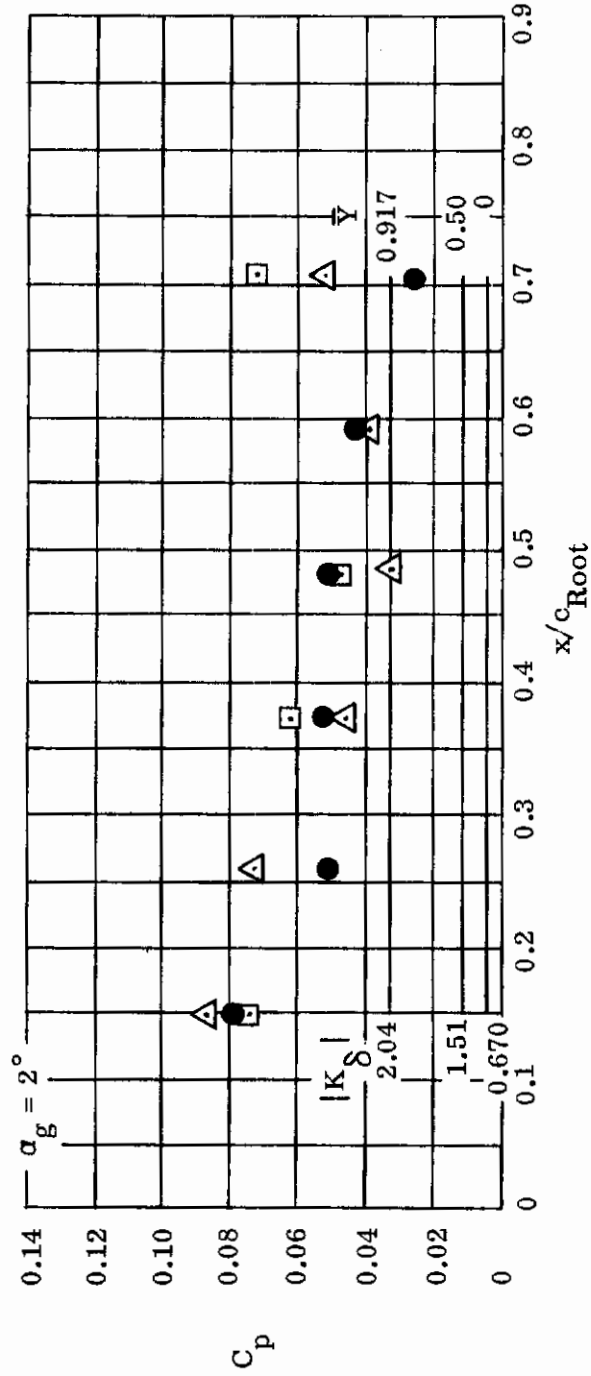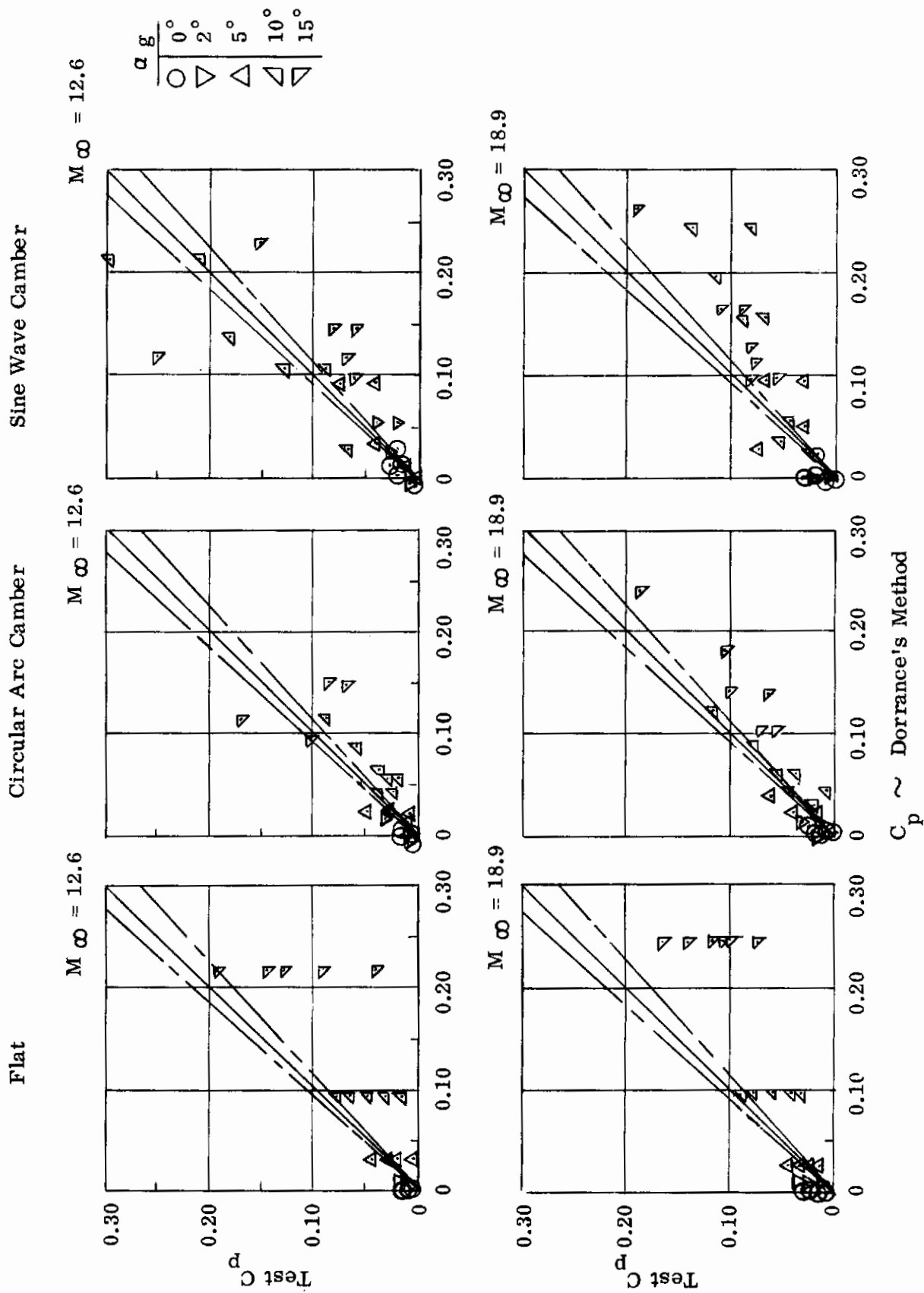
55

Figure 4.7. Theory to Test Comparisons Circular Arc Cambered Rectangular Wing $M_\infty = 19.2$, Dorrance's Method

Figure 4.8. Theory to Test Comparisons Twisted Rectangular Wing $M_\infty = 12.8$, Dorrance's Method
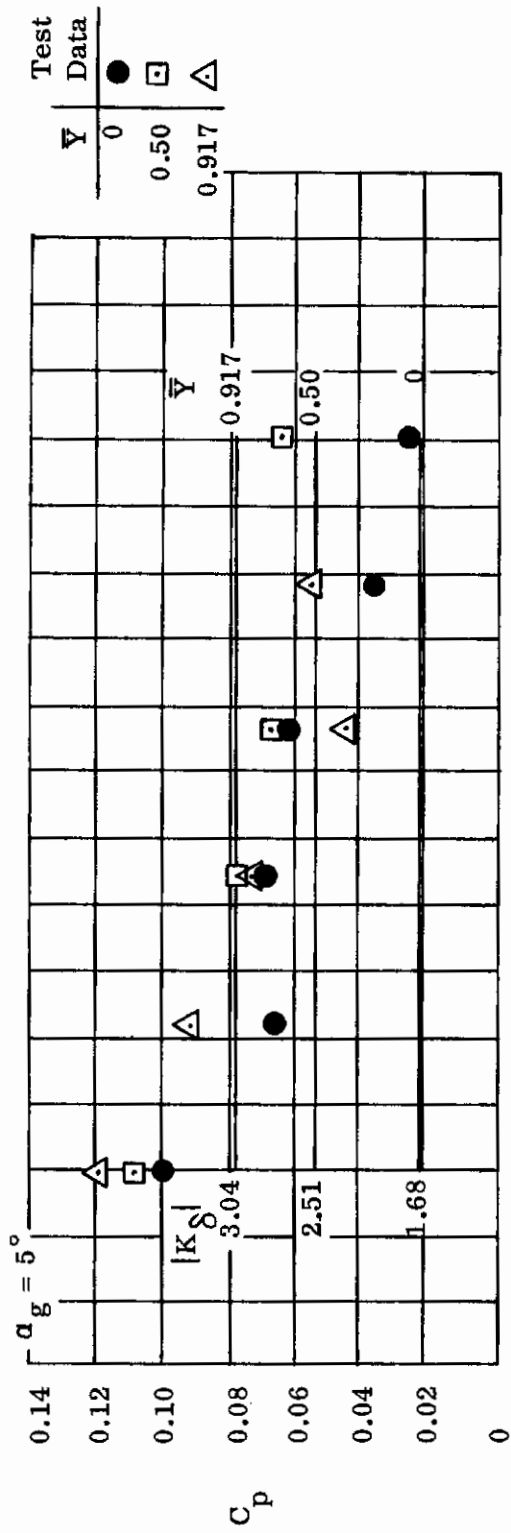
Figure 4.9. Theory to Test Comparisons Twisted Rectangular Wing $M_\infty = 19.2$, Dorrance's Method
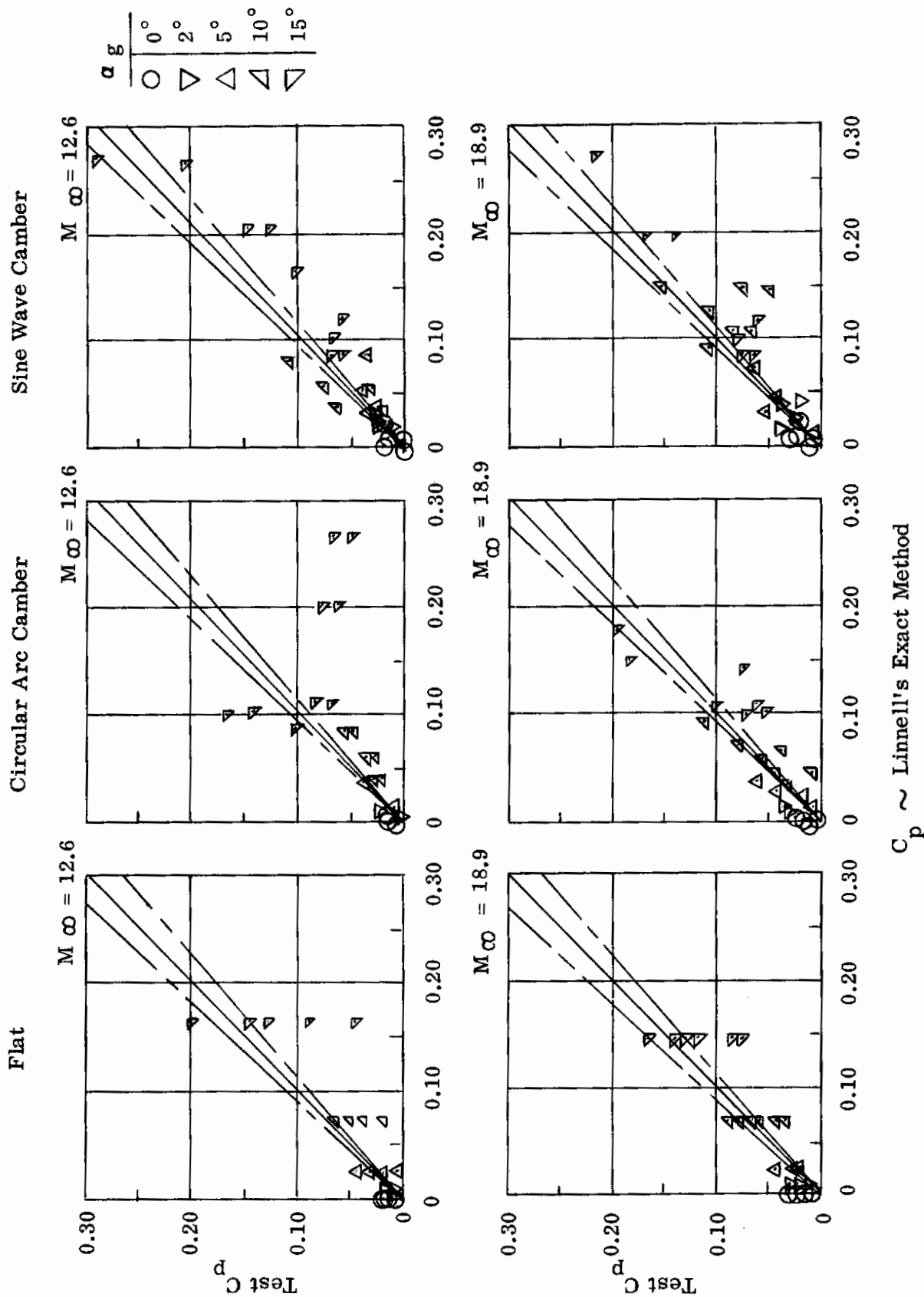
Figure 4.10. Theory to Test Comparisons - 70° Delta Wing

Figure 4.11. Theory to Test Comparisons - 70° Delta Wing
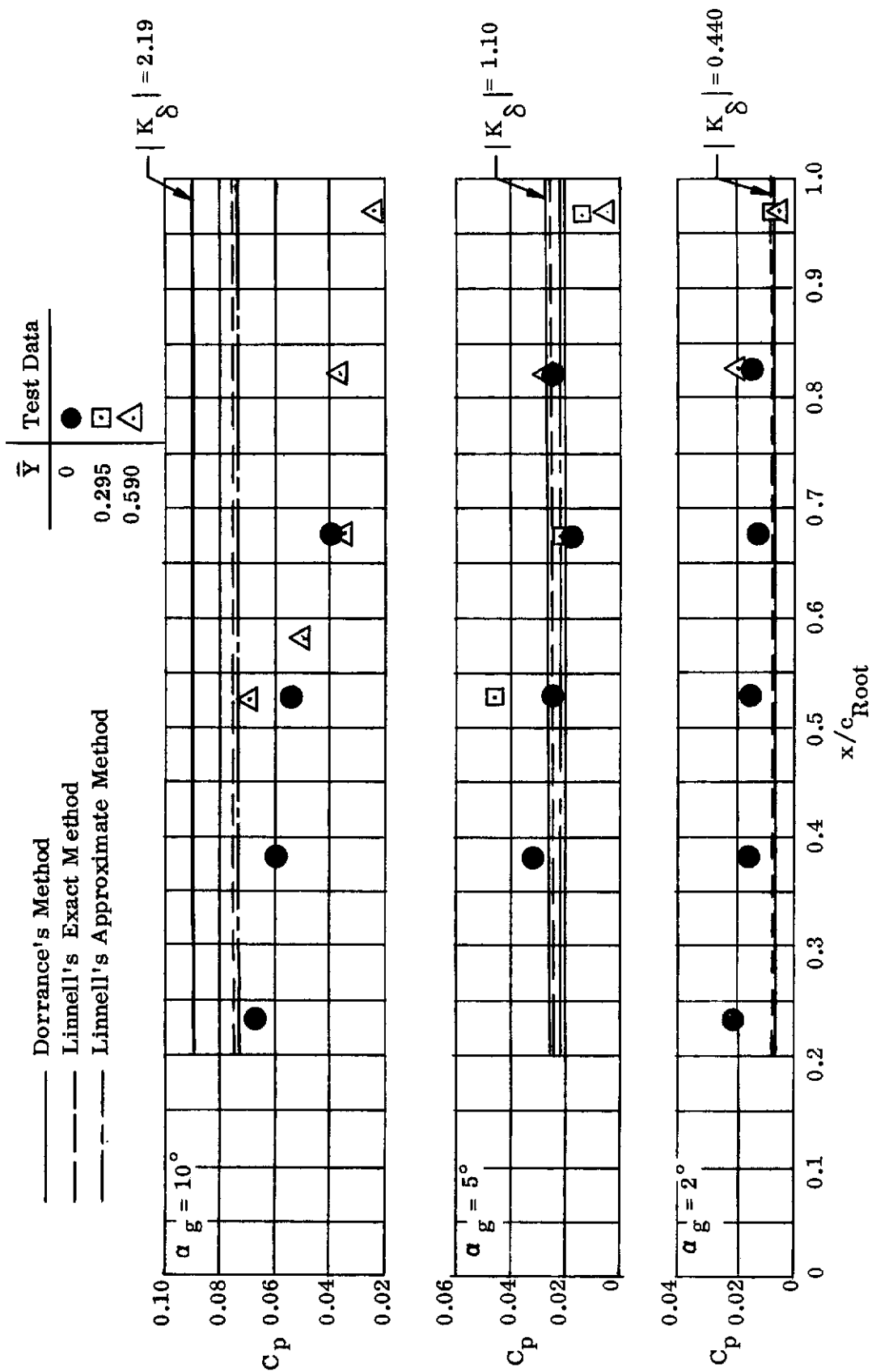
Figure 4-12. Theory to Test Comparisons, Flat 70° Delta Wing, $M_\infty = 12.6$
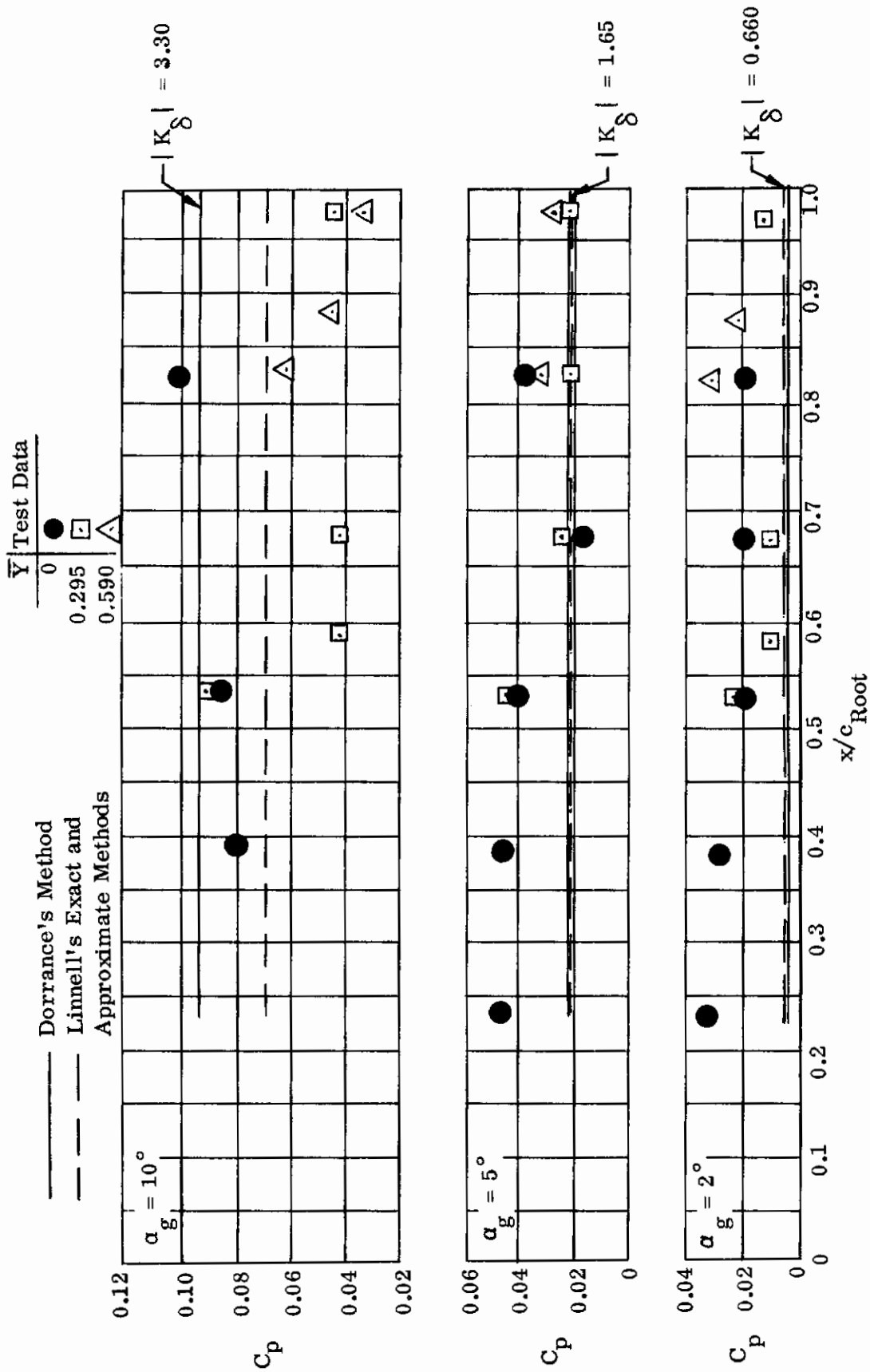
Figure 4.13. Theory to Test Comparisons, Flat 70° Delta Wing, $M_\infty = 18.9$
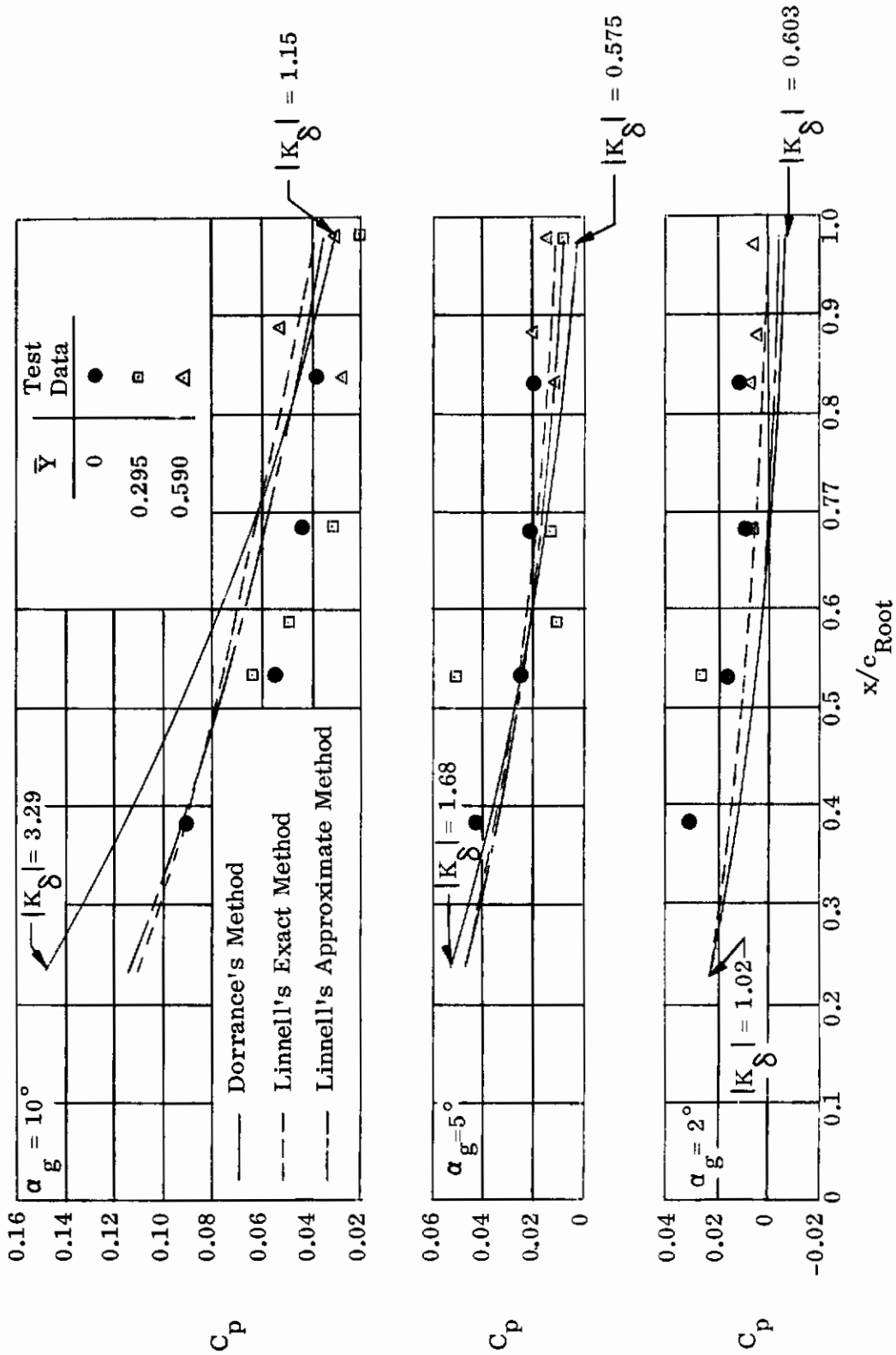
Figure 4.14. Theory to Test Comparisons Circular Arc Cambered 70° Delta Wing, $M_\infty = 12.6$

63
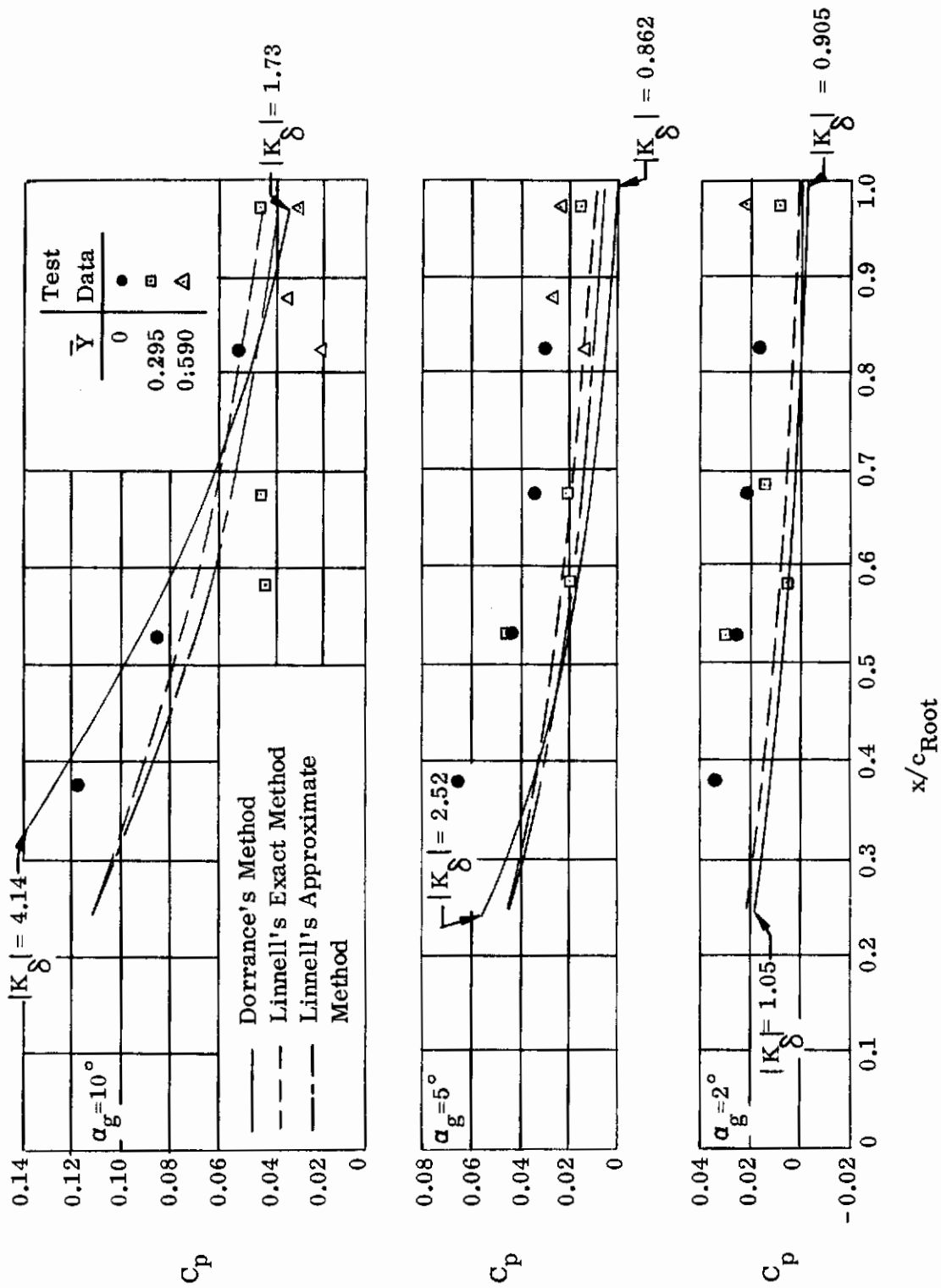
Figure 4.15. Theory to Test Comparisons – Circular Arc Cambered 70° Delta Wing M_∞ = 18.9
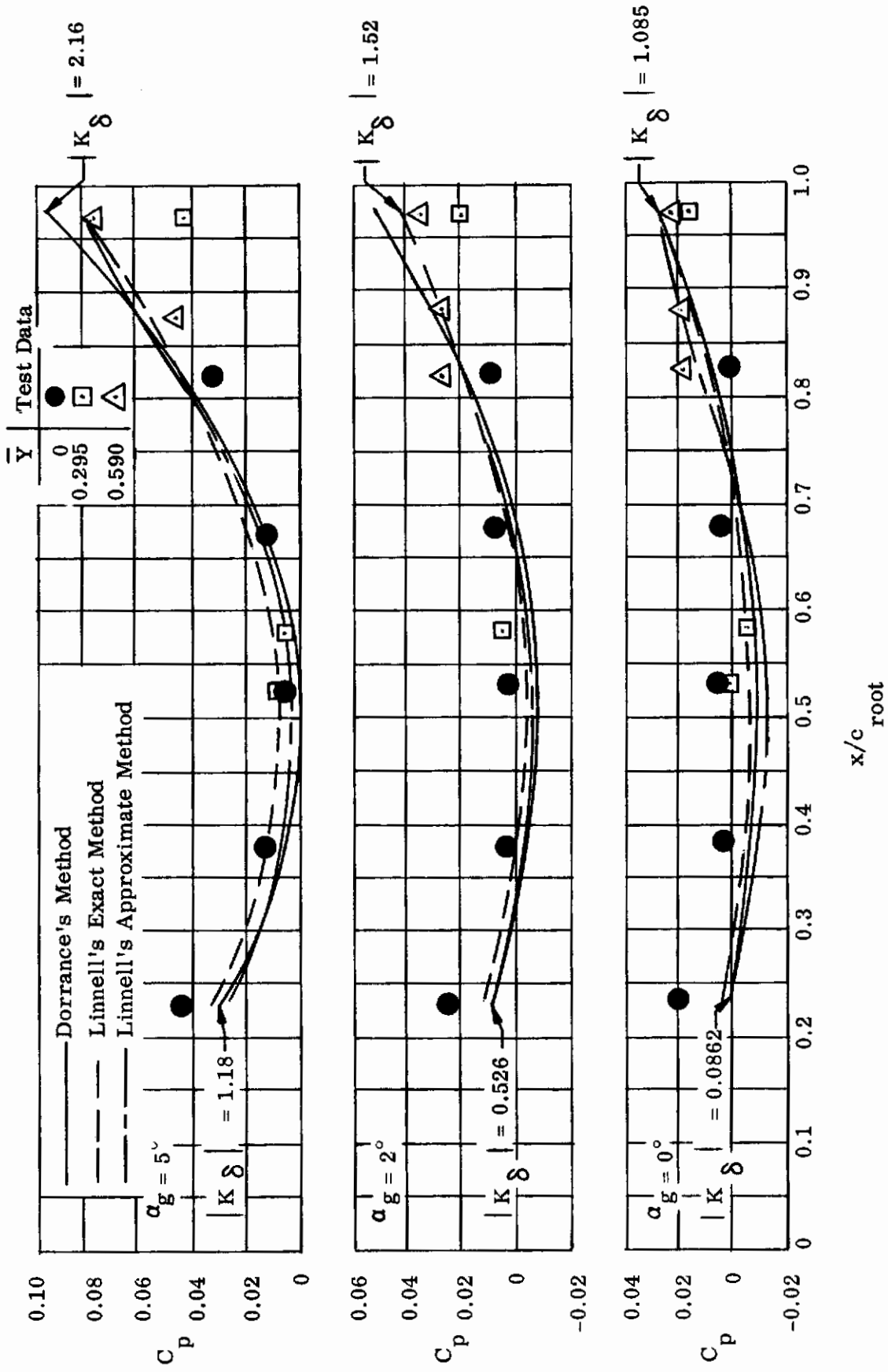
64

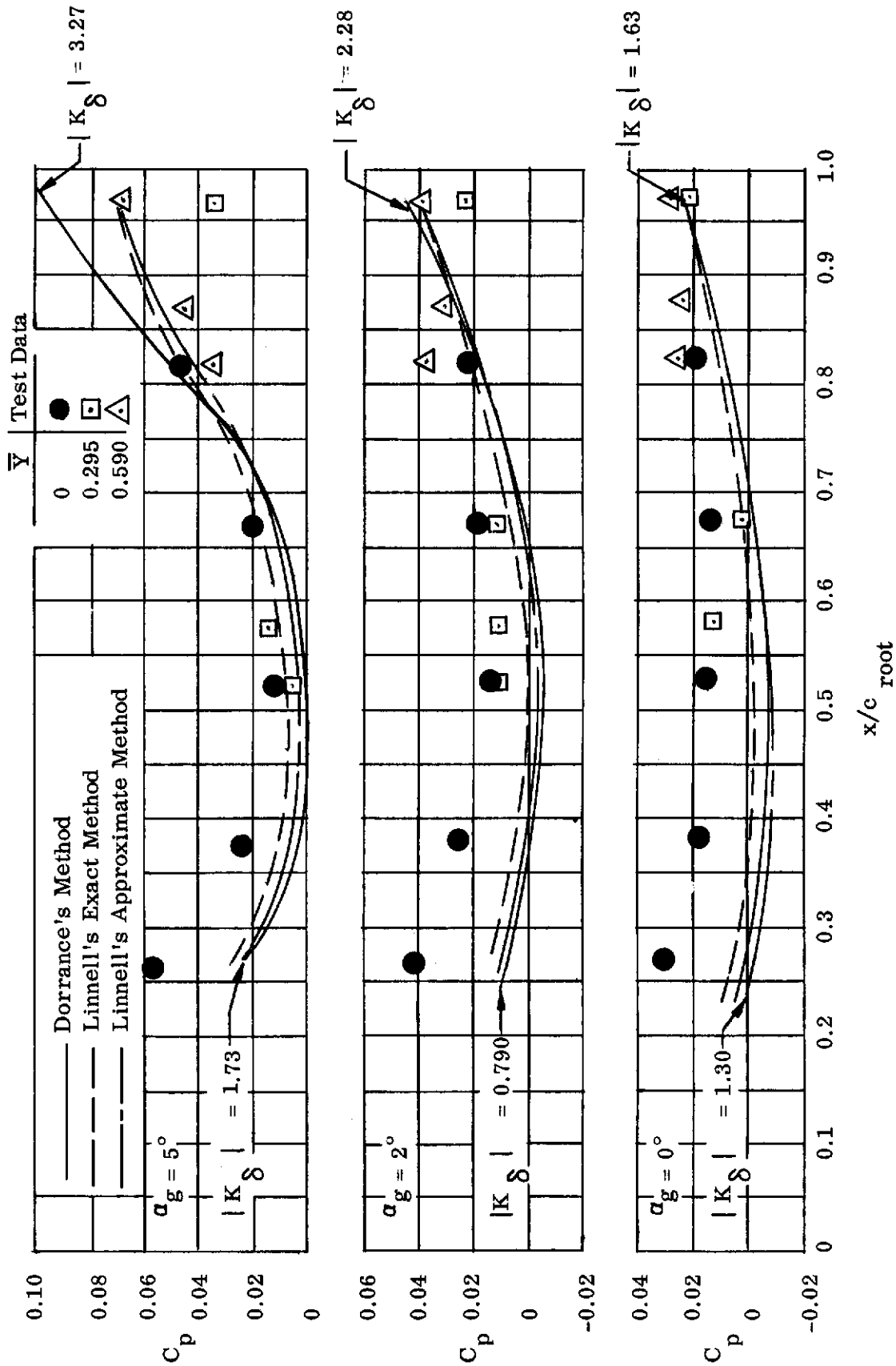Figure 4.16 Theory to Test Comparisons Sine Wave Cambered 70 Delta Wing, $M_\infty = 12.6$

65

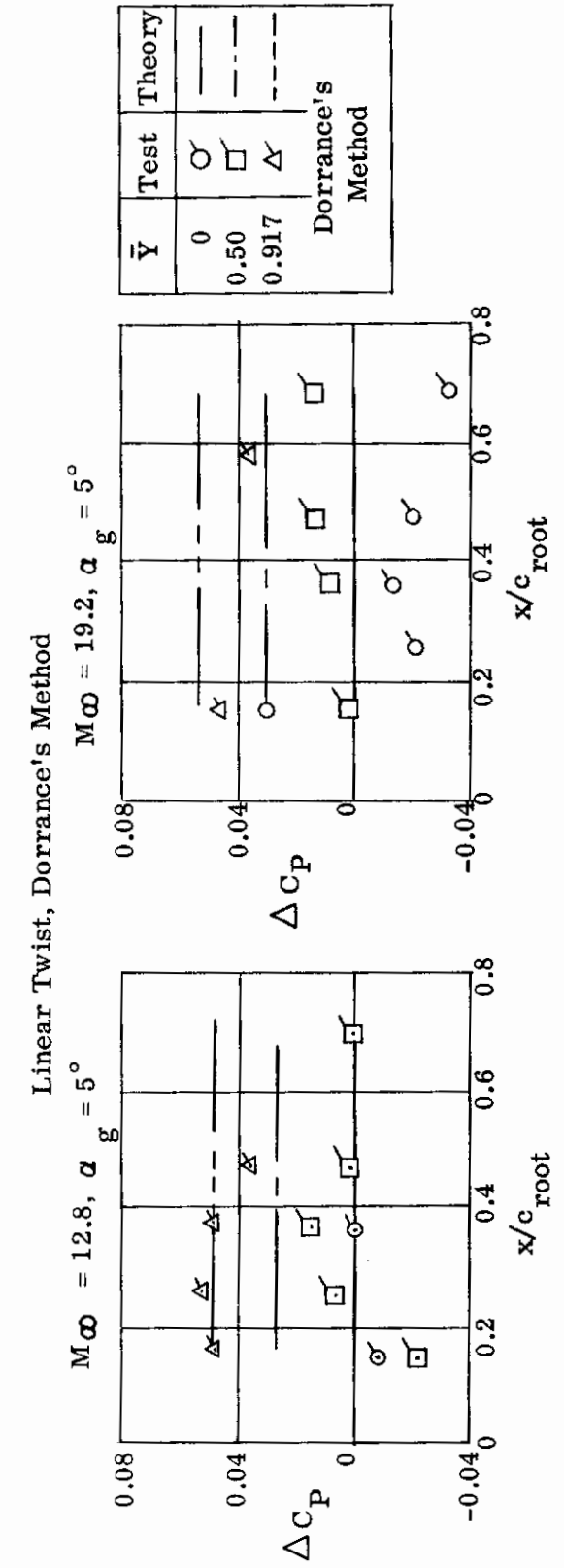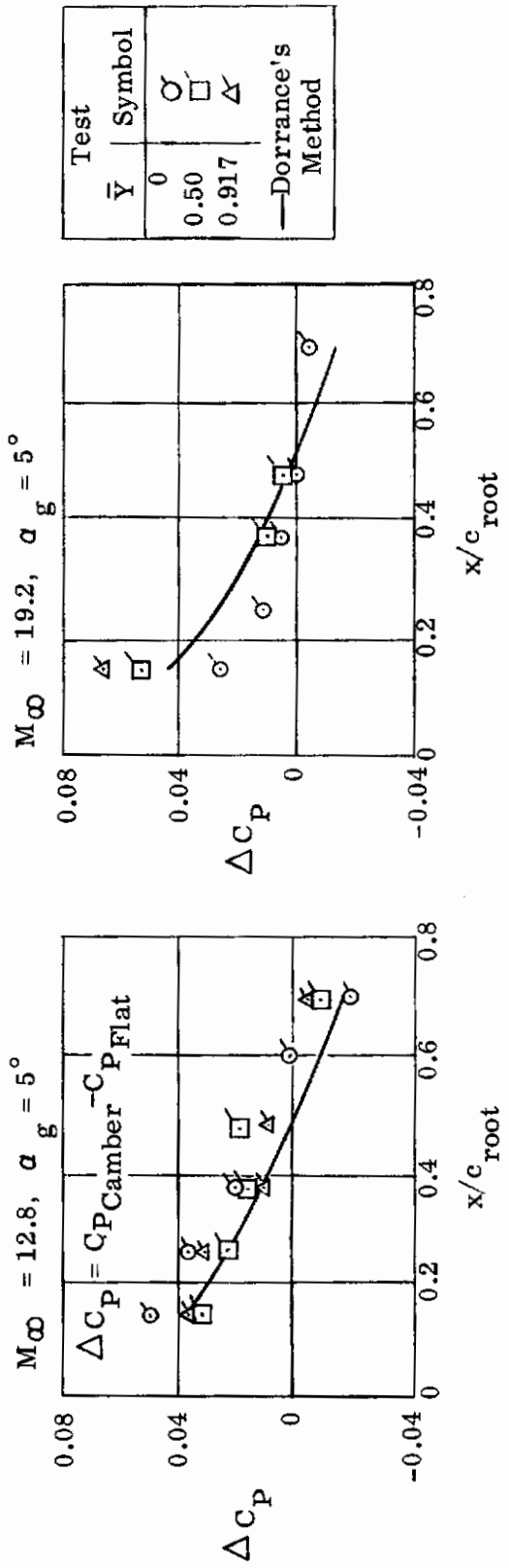Figure 4.17 Theory to Test Comparisons Sine Wave Cambered 70° Delta Wing, $M_\infty = 18.9$

Figure 4.18. Incremental Pressure Coefficients - Rectangular Wing
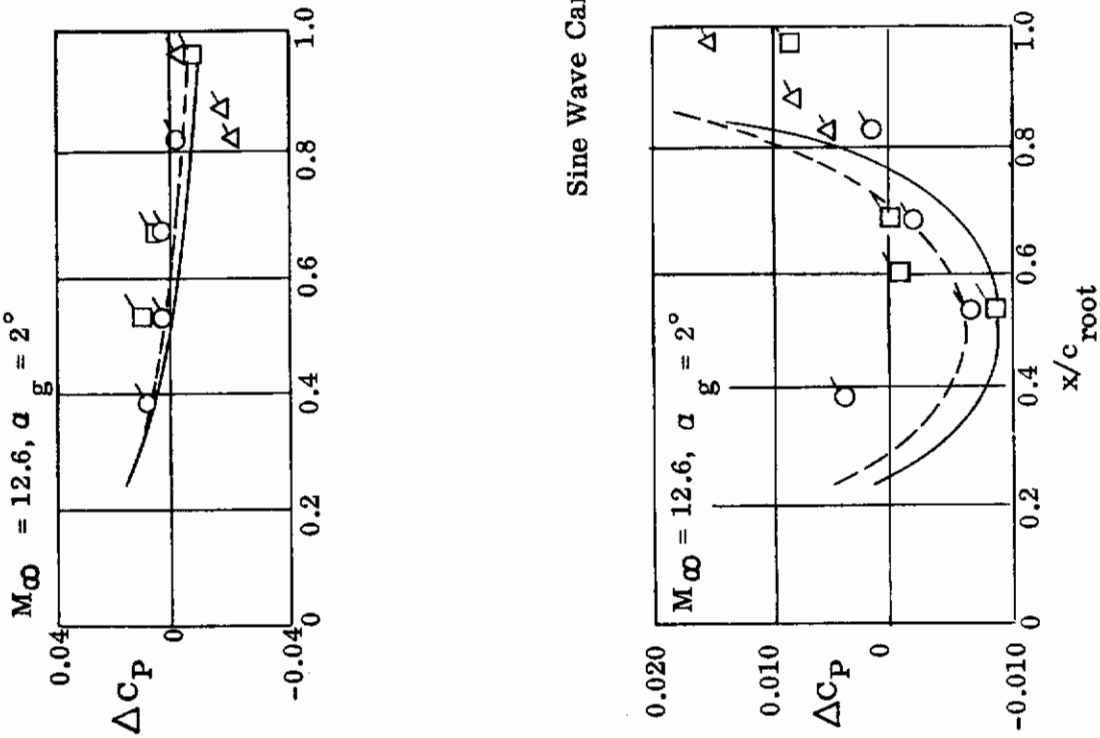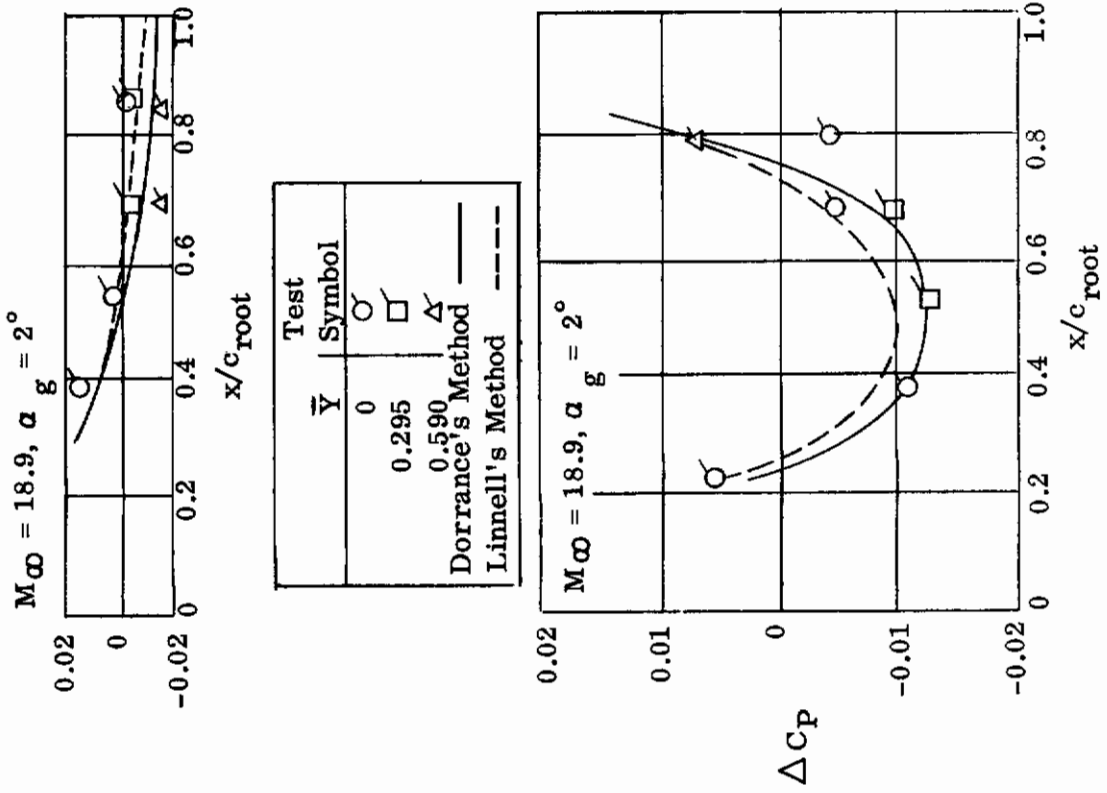
Figure 4.19. Incremental Pressure Coefficients –
70° Delta Wing

68

SECTION 5.0
SUMMARY

It became apparent during the studies reported in Reference 1 that no inviscid hypersonic pressure prediction method, expressed in influence coefficient form, was available for $\left| K_\delta \right| \geq 1.0$. The purpose of the subject study was to extend the range of application of the influence coefficients, (as expressed by $\left| K_\delta \right|$) by using an existing inviscid hypersonic pressure prediction method and in addition to evaluate the resultant aerodynamic influence coefficients by comparison with test data.

The range of application of the aerodynamic inputs developed in Reference 1 was extended by use of Linnell's pressure prediction method. Theoretically it was shown that this method is valid in the range $0 \leq \left| K_\delta \right| \geq 5.0$, however, one disadvantage of this method was uncovered. It was found that the lifting pressure for a flexible airfoil is a function, in addition to other parameters, of the unknown equilibrium angle of attack at the leading edge of the airfoil. It has been successfully demonstrated that by choosing $\alpha\,(0) = \alpha_g$ the problem is easily solved. Another method of solution is to iterate upon $\alpha\,(0)$ by programming Linnell's method as a subroutine in the nonlinear aeroelasticity FORTRAN program which is described in Part II of this report. Using this method aerodynamic operators would be calculated at each iteration for $\{\alpha\}$. The former method uses one known set of aerodynamic operators which are valid for all $\{\alpha\}$ iterations. The additional accuracy and loss in economy of the iterative method over the procedure derived in the present investigation is questionable in the light of the good results obtained using the present method. One certainty is that the iteration procedure described above would increase the complexity of the nonlinear aeroelasticity FORTRAN program.

Previous formulations of hypersonic aerodynamic influence coefficients (Reference 1) were easily obtained since lifting pressure relationships were polynomials in α. In the present study $\Delta p/q$ is a complex function involving algebraic

69

sums and products of powers of α . An accurate polynomial representation of $\triangle p/q$ was successfully obtained by applying a least-squares curve fitting technique to the complex α function. Volume 2 of this part of the final report presents aerodynamic influence coefficients using the approximate form of Linnell's method. These coefficients are presented graphically and have been devised so that only the pertinent parameters are shown. Unlike those developed in References 1, 13, and 14, the influence coefficients are a function of α_g, the rigid geometric angle of attack of the aerodynamic surface. Hence the Aeroelastician must not only take into account wing planform and cross-sectional shape, speed and altitude, but also the rigid angle of attack in order to determine $\left\lfloor Q_n \right\rceil$ matrices.

As with any theoretical method, it is desirable to assess its validity by comparison with test data. Both Dorrance's and Linnell's methods have been compared with pressure data measured on a series of warped and twisted wing models at hypersonic speeds. The test program was conducted by the Grumman Aircraft Engineering Corporation. Due to the fair agreement obtained between the theoretical methods and these particular test data no conclusive statements can be made in regards to the accuracy and range of validity of the hypersonic aerodynamic operators associated with these methods. Numerous results and conclusions based on the theory to test comparisons are given in Paragraph 4.5 of Section 4.0.

The pressure prediction methods and the associated influence coefficient matrices presented in Reference 1 were the first steps in detailing hypersonic aerodynamic operators for use in nonlinear static aeroelastic analyses. The work performed in the present study and presented in this part of the final report extends those methods developed in Reference 1.

SECTION 6.0

REFERENCES

1. Batt, J. R., Thermoelastic Effects on Hypersonic Stability and Control, Part I - "Hypersonic Aerodynamics" ASD TR 61-287, May 1963.

2. Gallagher, R. H. and Huff, R. D., Thermoelastic Effects on Hypersonic Stability and Control Part II, Volume I - "Elastic Response Determinations for Severely Heated Wings", ASD TR 61-287, August, 1962.

3. Quinn, J. F., Thermoelastic Effects on Hypersonic Stability and Control, Part II, Vol. II, "Elevated Temperature Deflection Influence Coefficient Tests of a Fuselage and a Combined Wing-Fuselage Structure", ASD TR 61-287, May, 1963.

4. Gallagher, R. H. and Huff, R. D.: Thermoelastic Effects on Hypersonic Stability and Control, Part II, Volume III, "Elastic Response Analysis of Fuselage and Combined Wing Fuselage Structures." ASD TR 61-287, May, 1963.

5. Padlog, J., Donato, V. W. and Batt, J. R., Thermoelastic Effects on Hypersonic Stability and Control, Part III "Hypersonic Aeroelasticity", ASD TR 61-287, May, 1963.

6. Batt, J.R. and R.H. Gallagher Nonlinear Thermoelastic Effects on Hypersonic Stability and Control, Part II, "Analytical and Experimental Static Aerothermo-elasticity", FDL-TDR-64-16, January 1964.

7. Padlog, J. and Gallagher, R.H., "Measurement of Angular Displacements of Practical Wing Structures by the Moire' Fringe Technique", FDL-TDR-64-42, January 1964.

8. Dorrance, W. H., "Two Dimensional Airfoils at Moderate Hypersonic Speeds," Journal of Aeronautical Sciences - Vol. 19, September 1952.

9. Linnell, R., "Two Dimensional Airfoils in Hypersonic Flow" Journal of Aeronautical Sciences, January 1949.

10. Hopkins, H. B., Scheuing, R. A., and Leng, J., Investigation of Pressure Distributions Over Planar, Twisted, and Cambered Wings In a Hypersonic Shock Tunnel, ASD TR 62-171, February 1962.

11. Eggers, A., Syverston, C. and Kraus, S., A Study of Inviscid Flow About Airfoils at High Supersonic Speeds, NACA TR 1123, 1953.

12. Donato, V. W., Supersonic Aeroelastic Effects on Static Stability and Control, Part III - "Aeroelastic Interaction", WADC TR 58-95, July 1960.

13. Zisfein, M. B., Donato, V. W., and Farrell, R. F. (Unclassified Title) Supersonic Aeroelastic Effects on Static Stability and Control, Part I - "Aerodynamics", Volumes I and II, WADC TR 58-95, December 1958 (Confidential).

14. Batt, J. R. and Farrell, R. F. (Unclassified Title) Thermal Effects on Static Aeroelastic Stability and Control, Part II - "Aerodynamics", Volumes I and II, WADC TR 58-378, December 1959 (Confidential).

15. Harrison, R., Least Squares Polynominal Fit, CLLSQ1 Lockheed Aircraft Corporation, SHARE District No. 116, California Division.

16. McLellan, C. H., Bertram, M. H., and Moore, J. A., An Investigation of Four Wings of Square Planform at a Mach Number of 6.9 in the Langley 11-Inch Hypersonic Tunnel, NACA Report 1310, 1957.